sustainability

MDPI

Article

Mathematical Modeling of Pilot Scale Olive Mill Wastewater Phytoremediation Units

Margarita A. Petoussi [1] and Nicolas Kalogerakis [1,2,*]

[1] School of Chemical and Environmental Engineering, Technical University of Crete, 73100 Chania, Greece
[2] Institute of GeoEnergy, Foundation for Research and Technology—Hellas (FORTH), 73100 Chania, Greece
* Correspondence: nkalogerakis@tuc.gr

Abstract: A mechanistic state–space model has been developed to describe the dynamics of olive mill wastewater (OMW) treatment in phytoremediation pilot units with *P. granatum* L. and *M. communis* L. plants and to assess further the relative contribution of the plants in the overall OMW remediation process. Both phytoremediation and bioremediation processes have been considered in the model, i.e., phytodegradation, rhizodegradation, accumulation of hardly biodegradable organic matter on the root tissue of plants, microbial growth, maintenance and decay, and enzymatic decomposition of organics. Maximum specific microbial growth rates for bacteria and fungi were estimated within the range of 0.164–0.236 1/h. The specific rate for the decomposition of hardly biodegradable organics both by bacteria and fungi was within the range of 10.75–72.73 mg-substrate/g-biomass·h, whereas, particularly for the high-molecular-weight polyphenols, it was 1.02–18.25 mg-substrate/g-biomass·h. The values of the transpiration stream concentration factor were greater than 0.95 for both the non-phenolic and phenolic organics, which indicates almost passive uptake of OMW organics' mixture by the plants. The corresponding factors for inorganic N and P were estimated as greater than unity, indicating active uptake. Overall, the model predicts the experimental data well when the organic concentration of OMW is high, and it predicts that phytoremediation processes contribute by more than 91% to the removal of OMW organics and nutrients, irrespective of the wastewater organic strength.

Keywords: olive mill wastewater; phytoremediation; mathematical modeling; polyphenols; *Punica granatum* L.; *Myrtus communis* L.

Citation: Petoussi, M.A.; Kalogerakis, N. Mathematical Modeling of Pilot Scale Olive Mill Wastewater Phytoremediation Units. *Sustainability* **2023**, *15*, 8630. https://doi.org/10.3390/su15118630

Academic Editors: Ana Luísa Ferreira Andrade Ramos and José António de Vasconcelos Ferreira

Received: 5 March 2023
Revised: 17 May 2023
Accepted: 23 May 2023
Published: 25 May 2023

1. Introduction

Olive mill wastewater (OMW) constitutes a complex wastewater with varying composition and high concentration of organics and nutrients. Recently, Mediterranean countries have individually permitted, through legislation, the direct disposal of non-treated OMW on soil [1] since no affordable and efficient treatment technology has been found to date for this type of wastewater. However, this practice imposes the risk of groundwater contamination and, at the same time, requires the use of vast land area. To eliminate the aforementioned drawbacks, Santori and Cicalini (2002) [2] introduced a phytoremediation scheme for OMW treatment by recirculation, where OMW was used as an irrigation source for planted soil in restricted areas. This technology was implemented successfully on a large scale in Italy, and the efficacy of tree-based phytoremediation for OMW treatment was well proven [3]. The main advantage of this technology against physicochemical and biological methods for OMW treatment is that it can be easily implemented (without technical expertise) in small decentralized olive mills with only a minor fixed cost for soil excavation, purchase of pumping and piping equipment, and the plants to be cultivated. Petoussi and Kalogerakis (2022) [4] recently proposed the use of high economic importance of plants in OMW phytoremediation to improve the circular economy character of the previous technology. They quantified the efficiency of the proposed technology in terms

of organic and nutrient removal rates and compared those rates with the corresponding removal rates of the relevant OMW-treating CWs. They also demonstrated, at the same time, the high contribution of the plants in the OMW treatment scheme. In the proposed treatment scheme, OMW constituents are removed both through processes related to bulk soil biomass activity, as well as through plant-related processes, such as plant uptake, rhizodegradation, and accumulation on plants' roots. However, the distinct contribution of each of the above processes to the overall remediation rate has not been quantified since there is no available model to describe this specific system.

To the best of our knowledge, no modeling work has been devoted yet to the description of the dynamics of OMW degradation on soil, although this practice is very common in most Mediterranean countries. In contrast, numerous studies have described thus far the simple kinetics of OMW remediation in small-scale bioreactors or sand columns [5–9]. The most recent literature on modeling related to OMW remediation includes studies on polyphenols recovery, whereby adsorption kinetics on various matrix materials are studied both experimentally and kinetically [10–12]. In addition, OMW flocculation–sedimentation and biological oxidation has been studied kinetically by Vuppala et al. (2019) [13], as well as co-metabolism of OMW in sequencing batch reactor under aerobic conditions after Fenton-based oxidation [14]. More complex integrated mathematical models on OMW remediation are scarce and have been so far developed for processes such as OMW composting [15,16] or for the incorporation of OMW polyphenols degradation in activated sludge systems [17].

The aims of the present study are to develop a mathematical model to adequately describe OMW degradation in a pilot phytoremediation system which uses tree species with high-value products and to determine the kinetics and the relative contribution of the various bioremediation and phytoremediation processes of the proposed system in the overall remediation of OMW. Moreover, since there are many studies for direct OMW application on bare soil, where OMW is applied in doses and gradually biodegraded, it is of interest to examine whether the presence of fruit-bearing deciduous shrubs provides an advantage in terms of the overall OMW degradation rates in addition to the economic advantage of cultivating attractively priced fruits (pomegranates or myrtle berries). Furthermore, mathematical modeling is an essential tool for the optimization of the pilot system's operation and the estimation of the contribution of other important variables of phytoremediation, such as the plants' root system development, concentration of rhizosphere microbial biomass, diversity of the plant species, and wastewater synthesis.

Innovative points in the model are the conceptual division of OMW organic mixture in two pools (labile and recalcitrant), whereby microbial biomass grows on both organic fractions following Monod as well as Haldane kinetics. Moreover, OMW polyphenol concentration has been considered as a separate state variable due to the profound importance of phenolics to the recalcitrant character of OMW.

2. Materials and Methods

2.1. Operation of the Phytoremediation Pilot Units

The model of the present study aimed to describe the operation of the phytoremediation system presented by Petoussi and Kalogerakis (2022) [4]. In the previous work, OMW was gradually remediated by recirculation through the soil in two sandy soil pilot units, each planted with two plants of either *Punica granatum* L. (pomegranate tree) or *Myrtus communis* L. (myrtle tree) species (Figure 1).

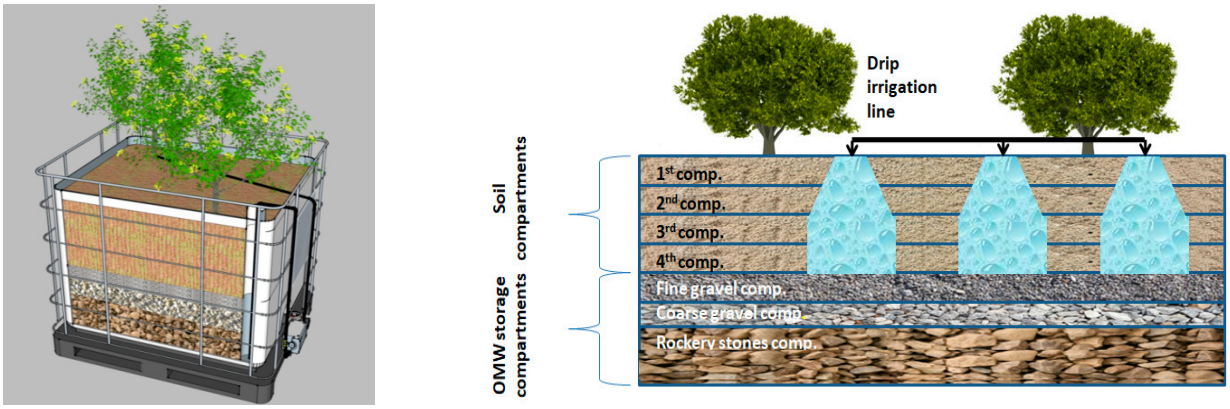

(**a**) (**b**)

Figure 1. (**a**) Schematic view of the phytoremediation pilot units and (**b**) compartments considered by the model.

Experimental data used for model calibration and validation were produced during four OMW treatment cycles performed during the summer months in two consecutive years. At the onset of each experimental cycle, both pilots were supplied with diluted OMW in the storage compartment, which subsequently was pumped continuously to the surface of the units for 12 h/d and infiltrated through the soil. Raw OMW had initial average chemical oxygen demand (COD) concentration for Cycles #1–#3 (1st year) and Cycle #4 (2nd year), corresponding to 2700, 6200, 12,400, and 39,300 mg/L, respectively. The dynamics of the most important OMW physicochemical variables, i.e., COD, biochemical oxygen demand (BOD_5), total polyphenols (TPh), total nitrogen (TN), and total phosphorus (TP), were investigated.

2.2. Model Development of the Phytoremediation Pilot Units

Due to the macroscopic character of the model, several assumptions were made to simplify hydrodynamics and mass transfer phenomena in the pilots. More specifically, the soil layer of the unit was conceptually divided into four equal-volume consecutive compartments (Figure 1b) in a tank-in-series approach [18] to account roughly for the plug–flow type of movement of the wastewater liquid phase through the soil. Assumptions on the characteristics of the plants' root system in the two pilots were based on the most relevant available information found in the literature and are described in detail in Appendix A.1.

OMW was provided to the surface of each unit by drip irrigation, where in sandy soil, the vertical water flow was reported to be much faster than the horizontal flow due to the high infiltration rate. Therefore, OMW was considered to be infiltrated only from a specific fraction of each unit's total soil (wetted soil region), shown schematically in Figure 1b. Numerical estimation of the mass of the total wetted soil region was described in detail by Petoussi and Kalogerakis (2022) [4], and its corresponding percent distribution in the unit was considered to be 15%, 25%, 30%, and 30% for the 1st to 4thcompartments, respectively. Wetted soil has been considered as the matrix for the bioremediation and phytoremediation processes. OMW degradation in the storage compartment was not considered.

The wastewater's gravitational flow through the soil of the unit was considered to be one-dimensional. Due to the intermittent irrigation of the unit, the wastewater flow was expected to take place both under saturated and unsaturated conditions and was considered to follow a combination of the Darcy–Buckingham model and the "tipping bucket" approach [19,20]; corresponding considerations as well as the wastewater volume balance of each compartment are provided in detail in Appendix A.2.

The total volume of the wastewater in the system was considered to be gradually reduced both through water evaporation and the plants' evapotranspiration; corresponding considerations are provided in detail in Appendix A.3. Solutes were considered to be

distributed between the solid phase (soil) and the liquid phase (soil solution). Moreover, the liquid as well as the soil phase of each compartment was considered to be homogenous. The adsorption of OMW constituents on the soil was modeled by the linear type adsorption isotherm. Convection was considered as the main mass transfer mechanism within the liquid phase due to intense irrigation. To avoid high computational complexity, the transport of solutes within the liquid phase through diffusion was not explicitly modeled. However, in order to account for the effect of the soil water content on the diffusion of soluble OMW substrates in the liquid phase and their availability to microbial biomass, an approximation of the solutes' diffusion in the soil solution was considered, as described in detail in Appendix A.4. The model considerations, particularly those concerning the wastewater oxygenation, are provided in Appendix A.5.

2.2.1. Model State Variables

OMW organic compounds, such as proteins, simple carbohydrates, and lipids, are easily degraded by microorganisms (i.e., labile), while those that are more resistant to decomposition organics, such as lignin, cellulose, and hemicelluloses [21], are partially degraded and transformed slowly [22]. Therefore, in the model, OMW total organic matter, determined by COD, was conceptually divided into two organics pools with respect to their biodegradability degree, i.e., readily biodegradable organic matter (RBOM), determined by BOD_5, and slowly biodegradable organic matter (SBOM), corresponding to the remaining organic fraction ($COD \backslash BOD_5$). Each of the two organic pools was further divided into two pools with respect to the presence/absence of the phenolic character of their compounds. Polyphenolic compounds, a class of OMW organics, are of special interest in OMW management due to their phytotoxic character. As a fact, polyphenolic substances found in OMW have a wide range of molecular weights (MW) [23], from simple monomeric phenols, such as tyrosol and hydroxytyrosol, to high polymerized polyphenols, such as tannins and anthocyanins [24]. High MW polyphenols are produced by partial oxidation and polymerization of simple phenols and are generally hardly degradable [25]; thus, their equivalent COD was considered in the model as the phenolic fraction of SBOM, while the equivalent COD of the low MW polyphenols was considered as the phenolic fraction of RBOM. The concentrations of high and low MW polyphenols of OMW (in gallic acid equivalents) were considered as model state variables (C_{HPh} and C_{LPh}), both comprising the total polyphenol (TPh) pool.

Eventually, OMW organics were considered in the model to be divided in the following pools: (a) non-phenolic SBOM, (b) phenolic SBOM, (c) non-phenolic RBOM, and (d) phenolic RBOM, where pools (a) and (c) corresponded to state variables $C_{S,NPh}$ and $C_{R,NPh}$, while (b) and (d) were determined as the equivalent COD concentrations of high and low MW polyphenols.

The non-biodegradable fraction of OMW was not considered since OMW is derived from edible matter [26]. Note that the SBOM fraction refers to both soluble recalcitrant organics and organics in particulate form.

OMW contains nitrogen mostly in organic form as amino acids, peptides, etc. [27], which, soon after OMW application on the soil, is considered to be mineralized and available for plant nutrition [27]. Therefore, OMW total nitrogen (TN) was also considered to comprise two pools, i.e., one of organic and one of inorganic nitrogen compounds, both modeled as state variables (C_{org-N} and C_{in-N}).

OMW phosphorus is found mainly in the inorganic form of phosphate salts [27–30], and, thus, only one phosphorus pool was considered as a state variable (C_P).

Additional state variables were considered for the adsorbed mass of non-phenolic SBOM ($S_{ads,S,NPh}$), high MW polyphenols ($S_{ads,HPh}$)), and organic nitrogen ($S_{ads,\ org-N}$) on plants' roots.

Moreover, OMW DO concentration (C_O), the volume of the soil solution in the wetted region of each soil compartment (V_k)), and the wastewater volume in the storage compartment were considered as state variables.

The bacterial (X_b) and fungal (X_f) microbial biomass concentration of bulk and rhizosphere soil were also considered as state variables. However, no specialized populations were considered to be involved in specific processes, such as nitrification, ammonification, or phenol degradation.

The general state variables, as described above, were considered for the different compartments of the system (Table 1), and the number of state variables totaled 73.

Table 1. List of state variables used in the model.

Variable	Unit	Description	Compartments
C_O	mg-O_2/L	Dissolved oxygen concentration	Soil solution of the wetted region of soil compartment (4 soil compartments) and stored OMW (storage compartment)
$C_{R,NPh}$	mg/L	Readily biodegradable non-phenolic organic matter concentration (BOD_5)	
$C_{S,NPh}$	mg/L	Slowly biodegradable non-phenolic organic matter concentration (COD)	
C_{HPh}	mg/L	High MW phenolic compound concentration (gallic acid)	
C_{LPh}	mg/L	Low MW phenolic compound concentration (gallic acid)	
C_{org-N}	mg-N/L	Concentration of nitrogen in organic form	
C_{in-N}	mg-N/L	Concentration of nitrogen in inorganic form	
C_P	mg-P/L	Concentration of phosphorus	
$S_{ads,S,NPh}$	mg-COD/kg-root tissue	Concentration of adsorbed mass of non-phenolic SBOM on plants' root tissue	Plants' root tissue (4 soil compartments)
$S_{ads,HPh}$	mg-gallic acid/kg-root tissue	Concentration of adsorbed mass of high MW phenolic compounds on plants' root tissue	
$S_{ads,\ org-N}$	mg-N/kg-root tissue	Concentration of adsorbed mass of nitrogen in organic form on plants' root tissue	
$X_{b,b}$	g-biomass/kg-soil	Bulk soil bacterial biomass concentration	Bulk soil of the wetted region (4 soil compartments)
$X_{f,b}$	g-biomass/kg-soil	Bulk soil fungal biomass concentration	
$X_{b,r}$	g-biomass/kg-soil	Rhizosphere soil bacterial biomass concentration	Rhizosphere soil of the wetted region (4 soil compartments)
$X_{f,r}$	g-biomass/kg-soil	Rhizosphere soil fungal biomass concentration	
V_k	L	Liquid phase volume for the kth compartment or OMW storage compartment	Soil solution of the wetted region (4 soil compartments) and stored OMW (storage compartment)

The general mass balance for the soluble constituents (concerning SVs 1 to 8 of Table 1) in the soil solution of the kth unit compartment is given by Equation (1).

$$\frac{d(C_{i,k}V_k)}{dt} + \frac{dS_{i,k}}{dt}M_k = Q_{k-1}C_{i,k-1} - Q_kC_{i,k} + R_{i,k,total} \quad (1)$$

where $C_{i,k}$ is the concentration of the ith constituent in the soil solution of the kth compartment (mg/L), V_k is the volume of the soil solution of the kth compartment (L), $S_{i,k}$ is the concentration of the ith constituent adsorbed on the soil of the kth compartment (mg/kg-soil), M_k is the wetted soil mass of the kth compartment (kg), and $R_{i,k,\ total} = \sum_j (\pm)\ R_{i,k,j}$ is the sum of removal and production rates of the ith constituent in the kth compartment (mg/h) through process j. Rates $R_{i,k,j}$ are presented in Sections 2.2.2 and 2.2.3, and their contributions in the mass balance of each SV is provided in Table A1 of Appendix A.6. For notation simplicity, soil compartment indicator k is omitted in the equations of the processes' rates.

Soil concentration of the ith soluble constituent $S_{i,k}$, is considered to follow the linear sorption isotherm at every time instant (Equation (2)).

$$S_{i,k} = K_{sd,i}C_{i,k} \quad (2)$$

where $K_{sd,i}$ (L/kg) is the partition coefficient of the ith constituent. Combining Equation (1) and Equation (2):

$$\frac{dC_{i,k}}{dt} = \frac{(Q_{k-1}C_{i,k-1} - Q_kC_{i,k} + R_{i,k,total})}{V_k + K_{sd,i}M_k} \quad (3)$$

Particularly for the dissolved oxygen, the closed mass balance of Equation (4) is considered only in case of waterlogged conditions, where wastewater oxygen is not replenished from the air in the soil pores; nevertheless, it is consumed as the wastewater infiltrates through the soil.

$$\frac{dC_{O,k}}{dt}V_k = Q_{k-1}C_{O,k-1} - Q_kC_{O,k} + \sum_j(\pm)R_{O,\,k,j} \quad (4)$$

where j denotes consumption by (a) microbial growth, (b) maintenance, and (c) removal by plants' transpiration.

For the adsorbed organic constituents on plants' root tissue and the microbial biomass, no exchange between soil layers was considered. Therefore SVs X_b and X_f (g/kg-soil) follow the growth kinetics given by Equation (5) and equivalently, the concentration of adsorbed organics on the root tissue of plants where: $S_{ads,i,}$ where i denotes non-phenolic SBOM, high MW phenols, and org-N and follows the kinetics described by Equation (28).

2.2.2. Bioremediation Processes

Microbial Growth

Organic compounds of OMW with high energy content induce a rapid short-term increase in the number of soil copiotrophic bacteria or r-selected species which comprise the first colonizers of the newly added organic matter in the soil [31]. This phenomenon (priming effect) is reported to last only a period of several weeks after organics application on soil [32], during which time the bacteria assimilate fast RBOM, gaining the advantage over fungi due to their faster growth rate. OMW phenolics, although usually referred as the main factor of OMW antimicrobial properties [33], also include simple molecules of low MW, such as phenolic acids, i.e., tyrosol or hydroxytyrosol, which comprise the majority of the OMW phenolic fraction [34] and have been shown to serve as a carbon source for microbial growth [35–39]. Fungi species are also reported to have an important role in the biodegradation of high-molecular-weight and recalcitrant organic compounds of OMW [5,40,41].

Heterotrophic bacteria and fungi were considered in the model to grow on both the phenolic and the non-phenolic fractions of the labile organic matter (RBOM), following additive kinetics. For the non-phenolic RBOM substrate (sugars, amino acids, etc.), Monod growth kinetics were considered, while for the phenolic fraction of RBOM, Haldane kinetics were followed in order to describe the growth on the inhibitory substrate. Growth limitation by nutrients (nitrogen and phosphorus) was also considered. Bacterial population was considered as facultative aerobic, and fungi were considered as obligatory aerobic, as are most soil fungi species. In aerobic conditions, Monod type oxygen limitation was considered, whereas in anoxic conditions, oxygen limitation followed the inverse Monod model. In anoxic conditions, NO_3^-−N was considered as an additional growth limiting nutrient since NO_3^-−N has the role of an electron acceptor in anoxic bacterial growth and is generally leaching from soil. NO_3^-−N concentration was not considered, however, as a state variable; instead, it was assumed as a constant fraction of inorganic nitrogen concentration. It is noted that the bacterial population is assumed to be capable of growing in both aerobic and anoxic conditions, according to the current oxic state of the soil. This simplification is also made in activated sludge models, ASM1 and ASM2 [42]. Decay of

the microbial biomass was also taken into account, which led to the replenishment of both the SBOM and organic nitrogen pool. Microbial growth rates are given below in Equations (5)–(10):

$$\frac{dX_b}{dt} = (\mu_b - d_b)X_b \quad (5)$$

where μ_b and d_b (1/h) denote the bacterial specific growth and decay rate, correspondingly. Bacterial growth follows additive kinetics, as given in Equations (6) and (7).

$$\mu_b = \mu_{max,b} \sum L_{b,i} \quad (6)$$

$$L_b = \begin{cases} f_{NPh}\varphi_{Mnd,b}\varphi_{O,b,aer}\varphi_{in-N,b}\varphi_{P,b} \\ f_{Ph}\varphi_{Hld,b}\varphi_{O,b,aer}\varphi_{in-N,b}\varphi_{P,b} \\ f_{NPh}\varphi_{Mnd,b}\varphi_{O,b,anox}\varphi_{NO_3,anox}\varphi_{in-N,b}\varphi_{P,b} \\ f_{Ph}\varphi_{Hld,b}\varphi_{O,b,anox}\varphi_{NO_3,anox}\varphi_{in-N,b}\varphi_{P,b} \end{cases} \quad (7)$$

where $\mu_{max,b}$ is the maximum specific bacterial growth rate, and L_b corresponds to the bacterial growth limitation factors for the following growth conditions: $L_{b,1}$ denotes aerobic growth on non-phenolic RBOM; $L_{b,2}$ denotes aerobic growth on phenolic RBOM; $L_{b,3}$ denotes anoxic growth on non-phenolic RBOM; and $L_{b,4}$ denotes anoxic growth on phenolic RBOM. All limitation factors φ are shown in Table A2 of Appendix A.6. f_{NPh} and f_{Ph} correspond to the fraction of non-phenolic and phenolic substrate of RBOM pool, respectively, and are considered to weight the contribution of each component of L_b to the total rate according to the availability of each substrate.

Phenolic RBOM was estimated stoichiometrically as the equivalent BOD_5 of the low MW phenolic concentration expressed in gallic acid equivalents. Moreover, it was implicitly assumed that both aerobic and anoxic growth prevailed at each soil layer according to the current oxygen level of the liquid phase.

The corresponding growth equations for fungi are:

$$\frac{dX_f}{dt} = \left(\mu_f - d_f\right)X_f \quad (8)$$

where μ_f and d_f (1/h) denote the specific fungi growth and decay rate, respectively.

$$\mu_f = \mu_{max,f} \sum L_{f,i} \quad (9)$$

$$L_f = \begin{cases} f_{NPh}\varphi_{Mnd,f}\varphi_{O,f,aer}\varphi_{in-N,f}\varphi_{P,f} \\ f_{Ph}\varphi_{Hld,f}\varphi_{O,f,aer}\varphi_{in-N,f}\varphi_{P,f} \end{cases} \quad (10)$$

where $\mu_{max,f}$ is the maximum specific fungi growth rate, and L_f are the fungal growth limitation factors, namely, $L_{f,1}$ denotes aerobic growth on non-phenolic RBOM and $L_{f,2}$ denotes aerobic growth on phenolic RBOM.

Microbial Decomposition and Removal of Organic Compounds

High MW SBOM is assumed to be firstly broken down through extracellular enzymatic decomposition both by bacteria and fungi (Equations (11)–(13)) in order to form bioavailable organic compounds, directly assimilable by microorganisms for growth and maintenance [43]. As a part of the total OMW organics, high MW polyphenols are also subject to microbial decomposition and have been reported to be gradually degraded to simple phenolics via first-order enzymatic processes after OMW application on soil [44].

The decomposition of OMW organic matter was herein modeled following the modeling approach of the hydrolysis process in ASM models [42], according to its classical definition, whereby "high molecular weight complex substances are broken down into simpler easily digestible molecules which are subsequently taken up for biomass build

up" [42]. Enzymatic decomposition was considered, therefore, as surface reaction occurring in close contact between the organisms which provided the hydrolytic enzymes and the slowly biodegradable matter. Moreover, enzymatic decomposition took place in both aerobic and anoxic environments, and although it is not considered to be related to the electron acceptor type, reduction of its rate under anoxic conditions was considered, as it is well described for the anoxic hydrolysis process [42].

Total decomposition rate of the *i*th compound $R_{i,dec}$ is given as the sum of the corresponding decomposition rates by bacteria $R_{i,b,dec}$ and fungi $R_{i,f,dec}$ (Equations (11)–(13)), where *i* accounts for the non-phenolic (*i*: S, NPh) or phenolic (*i*: HPh) pool of SBOM.

$$R_{i,dec} = R_{i,b,dec} + R_{i,f,dec} \quad (11)$$

$$R_{i,b,dec} = k_{dec,\,i,b} A_{lim,i,b} X_b \left(\varphi_{O,b,aer} + n_h \varphi_{O,b,anox} \varphi_{NO_3,anox}\right) M \quad (12)$$

$$R_{i,f,dec} = k_{dec,\,i,f} A_{lim,i,f} X_f \varphi_{O,f,aer} M \quad (13)$$

where $k_{dec,\,i,b}$ and $k_{dec,\,i,f}$ (mg-substrate/g-biomass·h) are the maximum enzymatic decomposition specific rates of the *i*th pool of SBOM for bacteria and fungi, correspondingly, n_h (dimensionless) is the reduction factor of enzymatic decomposition rate in anoxic conditions, and $A_{lim,i,b} = \frac{\frac{C^*_i}{X_b}}{k_X + \frac{C^*_i}{X_b}}$ and $A_{lim,i,f} = \frac{\frac{C^*_i}{X_f}}{k_X + \frac{C^*_i}{X_f}}$ are the dimensionless limiting factors for the decomposition process due to the surface limited kinetics. k_X corresponds to the saturation constant of the surface limitation terms.

Decomposed non-phenolic SBOM was assumed to contribute equally to the non-phenolic RBOM pool in terms of COD. The same consideration was made for the high MW polyphenols, contributing to the low MW phenolics pool. However, reverse polymerization of simple OMW phenols was also reported to take place [45], which could have possibly led to the underestimation of the real phenolic fraction of the low MW phenolic pool since secondary metabolites of low MW polyphenols can possess higher total antioxidant activity than the initial complex phenolic molecule. However, this could be anticipated by the fact that high MW polyphenols have been also reported to possess high antioxidant activity [46].

Non-phenolic RBOM is consumed during microbial growth according to Equation (14).

$$R_{R,NPh,growth} = \left(\mu_{max,b} \sum_{i\,=\,1,3} L_{b,i} \frac{X_b}{Y_{X_b/R,NPh}} + \mu_{max,f} L_{f,1} \frac{X_f}{Y_{X_f/R,NPh}}\right) M \quad (14)$$

where $Y_{X_b/R,NPh}$ and $Y_{X_f/R,NPh}$ (g-biomass/mg-BOD_5) are the bacterial and fungal biomass stoichiometric yields, respectively, on the non-phenolic organic matter. Simple low MW phenolics were also mentioned to be degraded and consumed under aerobic conditions as assimilable carbon substrate from a wide variety of bacteria and fungi species [35–39]. However, the inhibition of the polyphenols' biodegradation in pure and mixed cultures at high phenol concentrations is well reported in both aerobic and anaerobic environments [9,47]. Therefore, in the model we considered low MW polyphenol consumption by both bacteria and fungi during microbial growth under inhibition (Equation (15)).

$$R_{LPh,growth} = \left(\mu_{max,b} \sum_{i\,=\,2,4} L_{b,i} \frac{X_b}{Y_{X_b/LPh}} + \mu_{max,f} L_{f,2} \frac{X_f}{Y_{X_f/LPh}}\right) M \quad (15)$$

where $Y_{X_b/LPh}$ and $Y_{X_f/LPh}$ (g-biomass/mg-gallic acid) are the biomass yields on low MW polyphenols for bacteria and fungi, correspondingly ($Y_{X_y/LPh} = Y_{X_y/R,NPh}\, c_{f,PhBOD}$, where $c_{f,PhBOD}$ is the equivalent BOD_5 of gallic acid). RBOM is also consumed by microbial

biomass for maintenance energy (Equation (16)), i.e., the energy consumed for functions other than the production of new cell material.

$$R_{R,NPh,mainten} = \left(k_{m,b}X_b + k_{m,f}X_f\right)\frac{C^*_{R,NPh}}{C^*_{R,NPh} + C^*_{R,Ph}}M \quad (16)$$

where $k_{m,b}$ and $k_{m,f}$ (mg-substrate/g-biomass·h) are the maintenance coefficients for bacteria and fungi, correspondingly, defined by Pirt (1982) [48] as the minimum substrate consumption to maintain the cells. We also considered simple OMW phenolics to be consumed for microbial maintenance (Equation (17)).

$$R_{LPh,mainten} = \left(k_{m,b}X_b + k_{m,f}X_f\right)\frac{C^*_{R,Ph}}{C^*_{R,NPh} + C^*_{R,Ph}}\frac{1}{c_{f,PhBOD}}M \quad (17)$$

A fraction of the decayed microbial biomass, expressed by the dimensionless parameter r_d, is considered to contribute back to the non-phenolic SBOM pool (Equation (18)).

$$R_{S,NPh,decay} = r_d\left(d_b\frac{X_b}{c_{f,b,SBOM}} + d_f\frac{X_f}{c_{f,f,SBOM}}\right)M \quad (18)$$

where $c_{f,b,SBOM}$ and $c_{f,f,SBOM}$ are the conversion coefficients of decayed microbial biomass to non-phenolic SBOM based on stoichiometric calculations on the bacteria and fungi chemical formulae, respectively.

Microbial Transformation and Removal of Nitrogenous Compounds

In the model, two nitrogen pools were considered to be contained in OMW, i.e., one pool of inorganic and one of organic nitrogen. The inorganic nitrogen pool was assumed to be enriched with NH_4^+-N by mineralization of organic nitrogen through ammonification (Equation (19).

The ammonification process was taken into consideration in the model, since an increase of the ammonifying bacteria population is often reported in soils amended with OMW [49]. Ammonifiers were not modeled, however, as a discrete bacterial population, as was the case in ASM1 model [42]. Instead, it was assumed that the possible effect of the different population sizes and kinetics of ammonifiers was lumped in the corresponding process kinetics. Ammonification was modeled as a surface process, similar to organic decomposition (Equation (12)):

$$R_{org-N,amm} = k_{amm}A_{lim,org-N,b}X_b\varphi_{O,b,aer}M \quad (19)$$

where k_{amm}(mg-substrate/g-biomass·h) is the maximum ammonification specific rate, and $A_{lim,org-N,b}$ (dimensionless) is the surface limitation factor following the same formula as the corresponding factor for SBOM decomposition, as described in the previous section ($C^*_i = C^*_{org-N}$).

Nitrification of NH_4^+-N to NO_3^-−N was not modeled, instead NO_3^-−N was assumed to be a constant fraction of the inorganic nitrogen pool at every time instant. Our assumption was based on the results of many studies on OMW direct application on soil, whereby ammonia oxidizing and nitrifying autotrophic bacteria were reported to be slightly inhibited, and nitrification disruption was also reported [50,51]. Moreover, OMW was expected to have a low concentration of NO_3^-−N since, at the same time, the stimulation of the soil denitrifier population was reported [50,51], and NO_3^-−N is well known to be leaching in soils. Mineralized nitrogen is considered to contribute equally to the inorganic nitrogen pool and to be thereafter assimilated by bacteria, fungi, and plants. Removal of

inorganic nitrogen through incorporation to bacterial and fungal biomass (immobilization) is considered to follow Equation (20).

$$R_{in-N,growth} = \left(\mu_b \frac{X_b}{Y_{X_b/N}} + \mu_f \frac{X_f}{Y_{X_f/N}}\right) M \quad (20)$$

where $Y_{X_b/N}$ and $Y_{X_f/N}$ (g-biomass/mg-substrate) are the stoichiometric biomass yields on nitrogen for bacteria and fungi, respectively.

Moreover, the organic nitrogen pool is replenished by a fraction (r_d) of the decayed microbial biomass nitrogen (Equation (21)).

$$R_{org-N,decay} = r_d \left(d_b \frac{X_b}{Y_{X_b/N}} + d_f \frac{X_f}{Y_{X_f/N}}\right) M \quad (21)$$

Denitrification was not considered in the model since its contribution to nitrogen removal is negligible.

Microbial Removal and Precipitation of Phosphorus (P)

Generally, phosphorus can be removed from wastewater either by precipitation and/or adsorption or by microbial uptake [52]. OMW phosphorus was considered in the model as consisting of only one pool of available inorganic constituents, which can be assimilated from microbial biomass for build-up (Equation (22)).

$$R_{P,growth} = \left(\mu_b \frac{X_b}{Y_{X_b/P}} + \mu_f \frac{X_f}{Y_{X_f/P}}\right) M \quad (22)$$

where $Y_{X_b/P}$ and $Y_{X_f/P}$ (g-biomass/mg-substrate) are the stoichiometric biomass yields on phosphorus for bacteria and fungi, respectively.

Moreover, the chemical precipitation of P in the soil is considered to be a non-reversible first-order kinetics process (Equation (23)) [53]:

$$R_{P,prec} = k_{prec} C_P V_i \quad (23)$$

where k_{prec} (1/h) is the specific P precipitation rate.

Precipitation, however, is independent of P sorption and desorption to soil, and the latter processes were modeled separately by linear adsorption. Mineralization of organic phosphorus originating from the decomposition of the decayed microbial biomass was not considered to be significant in the short experimental period and, thus, was omitted.

Microbial Consumption of Oxygen

Oxygen is considered to be consumed via aerobic microbial growth (Equation (24)) and maintenance (Equation (25)):

$$R_{O,growth} = \left(\mu_{max,b} \sum_{i=1,2} L_{b,i} \frac{X_b}{Y_{X_b/O}} + \mu_f \frac{X_f}{Y_{X_f/O}}\right) M \quad (24)$$

where $Y_{X_b/O}$ and $Y_{X_f/O}$ (g-biomass/mg-substrate) correspond to the stoichiometric biomass yields on oxygen for bacteria and fungi, respectively.

$$R_{O,mainten} = \left(k_{m,b} \varphi_{O,b,aer} X_b + k_{m,f} X_f\right) M \quad (25)$$

2.2.3. Phytoremediation Processes

Plant Uptake of Organic and Inorganic Compounds

Plants uptake organic contaminants passively from the soil solution during their transpiration [54]. The uptake efficiency is affected by the physical and chemical properties of the organic pollutants, i.e., the molecular mass and hydrophobicity, as well as by the biological characteristics of the plants and the environmental media. The molecular mass of organic pollutants has been reported as an important factor influencing the plant-uptake process, whereby compounds with molecular mass below 1000 can be easily absorbed by plant roots [55]. Therefore, sugars and proteins of OMW, which have mainly low-molecular mass, and the most abundant low-molecular-mass polyphenols in OMW, i.e., tyrosol and hydroxytyrosol [24], should also be considered to be taken up by plants [46].

Plants have also been known to uptake phosphorus in orthophosphate form [56] and nitrogen in both inorganic and organic form [57]. Inorganic nutrients are known to be taken up actively due to plant-induced gradients that drive them towards the roots [58].

In order to model the uptake of solutes (organics and nutrients) by plants, we herein adopted the approach of transpiration stream concentration factor (TSCF), which was proposed by Briggs et al. (1982) [59] as an indirect measure of the uptake efficiency. It is defined as: TSCF = Concentration in transpiration stream (mg/L)/Concentration of external solution in contact with root tissues (mg/L). According to Manzoni et al. (2011) [58], the plant uptake rate of both organic and inorganic compounds may be approximated simply as proportional to the mean transpiration rate and the compounds' concentration in the soil solution following Equation (26).

$$R_{i,uptake} = TSCF_i q_{ET} C_i \quad (26)$$

where i denotes non-phenolic RBOM, LPh, in-N, org-N, and P. The TSCF has a maximum value of 1 for passive uptake. TSCF factors larger than 1 indicate that nutrients have been moved against their concentration gradient [60]. Oxygen has also been considered to be taken up by plants passively, as contained in the evapotranspirated stream of the wastewater. In this type of model, plant uptake is effectively a "sink" process or loss mechanism for chemicals in the soil, and the eventual fate of the compounds within the plant is not investigated.

Accumulation of Recalcitrant Organics to the Plants' Root Zone

High-molecular-mass organic pollutants, which possess strong hydrophobic properties, are considered to be adsorbed on plant roots [55]. The potential of a given xenobiotic to accumulate on the plant root is described by the Root Concentration Factor (RCF), defined by Briggs et al. (1982) [59] as the ratio of the organic compound sorbed on the root (mg/kg-fresh root tissue) to the compound concentration in the soil solution (mg/L). Therefore, organic accumulation on plants' roots has been modeled according to Equation (27).

$$R_{i,ads} = k_{ads}(RCF_i C_i - S_{ads,i}) m_{tissue} \quad (27)$$

where k_{ads} (1/h) is the specific rate of adsorption on roots, and RCF_i (mg-substrate/kg-root tissue)/(mg/L) is the root concentration factor of constituent i: non-phenolic SBOM, high MW phenols, and org-N.

Rate of change of accumulated mass on the plants' root tissue is given by Equation (28).

$$\frac{dS_{ads,i}}{dt} = R_{i,ads}/m_{tissue} \quad (28)$$

Organics while sorbed on roots are not considered to be biodegraded and are subsequently backwashed to the soil solution according to the adsorption potential.

Rhizodegradation of Organic Compounds

Rhizodegradation refers to the breakdown of contaminants within the plant root zone, or rhizosphere. The rhizosphere is a microhabitat around roots, typically extending 1–2 mm around them [61], where an enhanced number and variety of microorganism species (bacteria and fungi) can be found. This "rhizosphere effect" is caused by the physical (i.e., gas exchange and soil moisture) and chemical (root exudates) impact of plant roots on the soil [54]. Rhizosphere microbial population concentration generally varies from 10- to 1000-fold with respect to bulk soil microbial biomass concentration [62]. Although no experimental assessment of the rhizosphere microbial population in the pilots was available, rhizodegradation could not be neglected in the model. Therefore, the rhizosphere microbial biomass concentration was modeled assuming additional state variables to describe the bacterial and fungal population in each of the 4 different soil compartments. The initial rhizosphere fungal and bacterial biomass concentration in the pilots was assumed to be two orders of magnitude greater than the corresponding concentration of the bulk soil. Since this assumption was highly uncertain, it was further examined in the sensitivity analysis of the model. It is noted also that rhizosphere bacterial and fungal biomass were considered to follow the same bioprocesses and relevant kinetics with the corresponding bulk populations. The mass of the total rhizosphere soil in the experimental period of the first year was estimated as 10% of the total wetted soil region of each pilot (20% for second year); this was estimated according to the calculation of the soil volume surrounding roots based on available information about the plants' root length distribution [63]) and the corresponding rhizosphere activity length [64]. The total mass of rhizosphere soil was distributed to the four unit layers according to the root distribution profile of each plant species. No additional rhizosphere soil compartments were considered in the model, for simplicity reasons. Due to the fast wastewater infiltration through the soil, it was assumed that the concentration of solutes in the soil solution of the bulk and the rhizosphere soil were the same.

2.3. Model Inputs and Parameters

The parameters of the model to be calibrated are related to the processes of (a) plant uptake, (b) adsorption on plants' roots, (c) microbial growth, (d) enzymatic decomposition of organics, and (e) phosphorus precipitation. These are correspondingly (a) transpiration stream concentration factors $TSCF_i$ (i denotes non-phenolic RBOM, low MW phenolics, in-N, org-N, and P), (b) root concentration factors RCF_i(i denotes non-phenolic SBOM, high MW phenolics, and org-N) and adsorption-specific rate constant k_{ads}, (c) maximum specific microbial growth rates $\mu_{max,y}$ (y denotes bacteria and fungi), semi-saturation constants $K_{S,i,y,}$(i denotes non-phenolic RBOM, phenolic RBOM, in-N, and P; and y denotes bacteria and fungi), semi-saturation constant $K_{S,NO3,b}$ for $NO_3{}^-N$ in anoxic growth conditions, and inhibition constants for phenolic RBOM $K_{S_i,R,Ph,y}$ (y denotes bacteria and fungi), (d) factor of enzymatic decomposition rate reduction in anoxic conditions n_h, enzymatic decomposition specific rates $k_{dec,i,y}$ (i denotes non-phenolic SBOM and high MW phenolics; and y denotes bacteria and fungi), and ammonification specific rate k_{ammon}, and (e) phosphorus precipitation specific rate k_{prec}. Units of the model inputs and the kinetic parameters to be calibrated are provided, correspondingly, in Tables A3 and A4 of Appendix A.6.

2.4. Model Calibration Methodology

The mechanistic model of the present study was developed in MATLAB® in state–space form. The governing differential equations were solved by MATLAB's ode15s differential equation solver. The model calibration was based on the available experimental data series of BOD_5, COD, TPh, TN, and TP concentrations of the recirculating OMW from Treatment Cycles #1 and #4 (i.e., treatment of low- and high-organic-strength OMWs, correspondingly) as well as the data of soil concentrations of bacterial biomass, total organic carbon (TOC), and TN measured at the end of the second experimental year given by Petoussi and Kalogerakis (2022) [4]. The corresponding data from Cycles #2 and

#3 (treatment of medium-organic-strength OMW) were used for model validation. Due to the different soil environments created by each plant species, the calibration procedure was conducted separately for the two phytoremediation pilot units. The calibration was performed according to the adaptive LJ optimization procedure [65], which uses random search points and systematic contraction of the search region. According to this method, an initial guess $k(0)$ of the p-dimensional unknown parameter vector (p = 29) was made and the initial search region was set as $r(0) = k_{max} - k_{min}$. The sum of the normalized root mean square errors (NRMSEs) of the experimentally defined variables was considered as the objective function to reflect the agreement of model prediction with measured data (Equation (29)):

$$NRMSE_{tot} = \sum_{j=1}^{Npm} NRMSE_j = \sum_{j=1}^{Npm} \left[\frac{1}{\overline{O_j}} \sqrt{\frac{1}{N_j} \sum_{i=1}^{N_j} (O_{ij} - P_{ij})^2} \right] \quad (29)$$

where Npm is the total number of experimentally measured variables, N_j is the total number of experimental data points available for the jth variable, O_{ij} and P_{ij} are the measured and corresponding predicted values, respectively, by the model for the ith experimental data point of the jth variable, and $\overline{O_j}$ is the mean value of the measured experimental data points. The number of random evaluations of the objective function within an iteration was set to 100, while the maximum number of iterations was set to 40, with a contraction of the search region at the end of each iteration by 95%.

3. Results and Discussion

3.1. Model Calibration

3.1.1. Simulated Dynamics

The simulated dynamics of OMW organic concentration during Cycle #1 and Cycle #4 for the two experimental units are shown in Figure 2.

The model follows satisfactorily the datasets of COD (Figure 2C,G) and TPh (Figure 2D,H) concentrations for both units during Cycle #4 (NRMSE equals 24% and 8% for *P. granatum* and *M. communis* pilots, correspondingly), where OMW of high organic strength is treated. On the contrary, during Cycle #1, COD and TPh concentrations are predicted with a high bias (average NRMSE for both units is equal to 78%) from the corresponding datasets (Figure 2A,B,E,F). The divergence of the model prediction from the data is due primarily to the limitation of the microbial growth by the lack of nutrients since labile organic matter is available throughout the entire experimental period of Cycle #1. During the last days of Cycle #1, the model also tends to increase the COD concentration on the basis of (a) the assumption of redissolution of organic matter concentrated in the plants' roots back to the soil solution and (b) the replenishment of the SBOM pool by the decayed biomass. As a fact, the model predicts less accurately the system dynamics during the treatment of low organic strength wastewater. From a process-related view, this also could be attributed to the promotion of organics enzymatic degradation in highly diluted OMW [25], which is not included mechanistically in the model.

Data regarding TN and TP concentrations are generally in high agreement with the model dynamics (Figures S3 and S4) for both units and cycles.

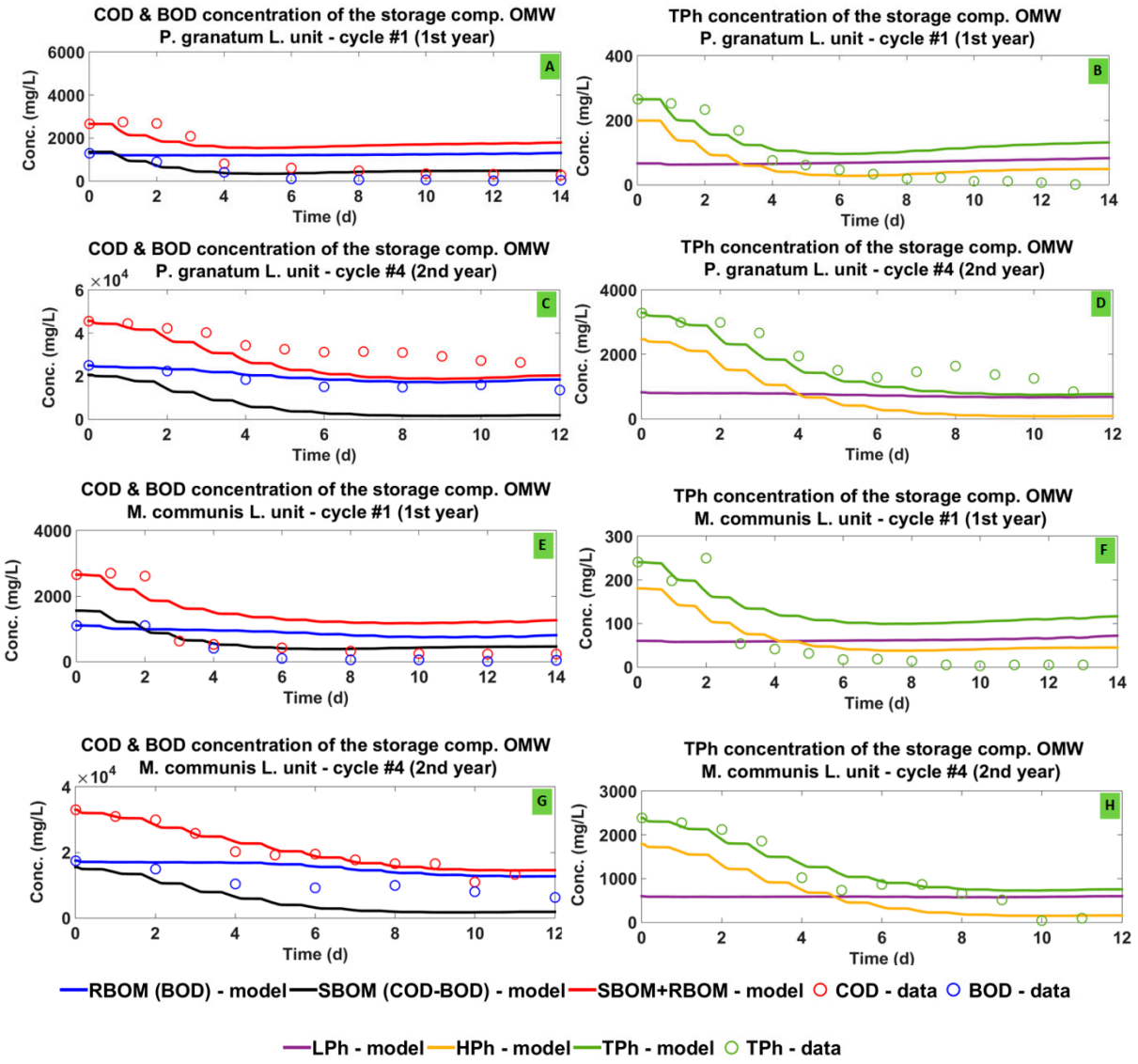

Figure 2. Dynamics of COD, BOD_5, and TPh concentrations of OMW in the storage compartment of (**A**–**D**) *P. granatum* and (**E**–**H**) *M. communis* plants unit during Cycles #1 and #4 of the experiment.

The simulated dynamics of soil bacterial biomass, TOC, and TN concentrations are given in Figure 3 for both the bulk and rhizosphere soil for *M. communis* (Figure 3A–C) and *P. granatum* units (Figure 3D–F) during Cycle #4.

Similar dynamics for rhizosphere and bulk soil microbial populations result from the fact that the same substrate availability and growth kinetics have been considered for the two populations. Bacterial biomass concentration (Figure 3A,D) increases initially due to the soil priming effect caused by the application of OMW organic matter, as also described by Kotsou et al. (2004) [31]. However, although labile organic matter is highly available up to the end of Cycle #4 (Figure 2C,G), the bacterial biomass concentration, especially in the *P. granatum* unit soon after the beginning of the cycle, follows a decreasing trend. This is due to the simultaneous substrate consumption by fungi and to the multiple nutrient limitation of the microbial growth. At the end of Cycle #4, there is a perfect match of the model prediction with data for the bacterial biomass in both units. Simulated dynamics of fungal biomass concentration are given as Supplementary Materials (Figures S8 and S9) since no corresponding experimental data were available for model calibration or validation.

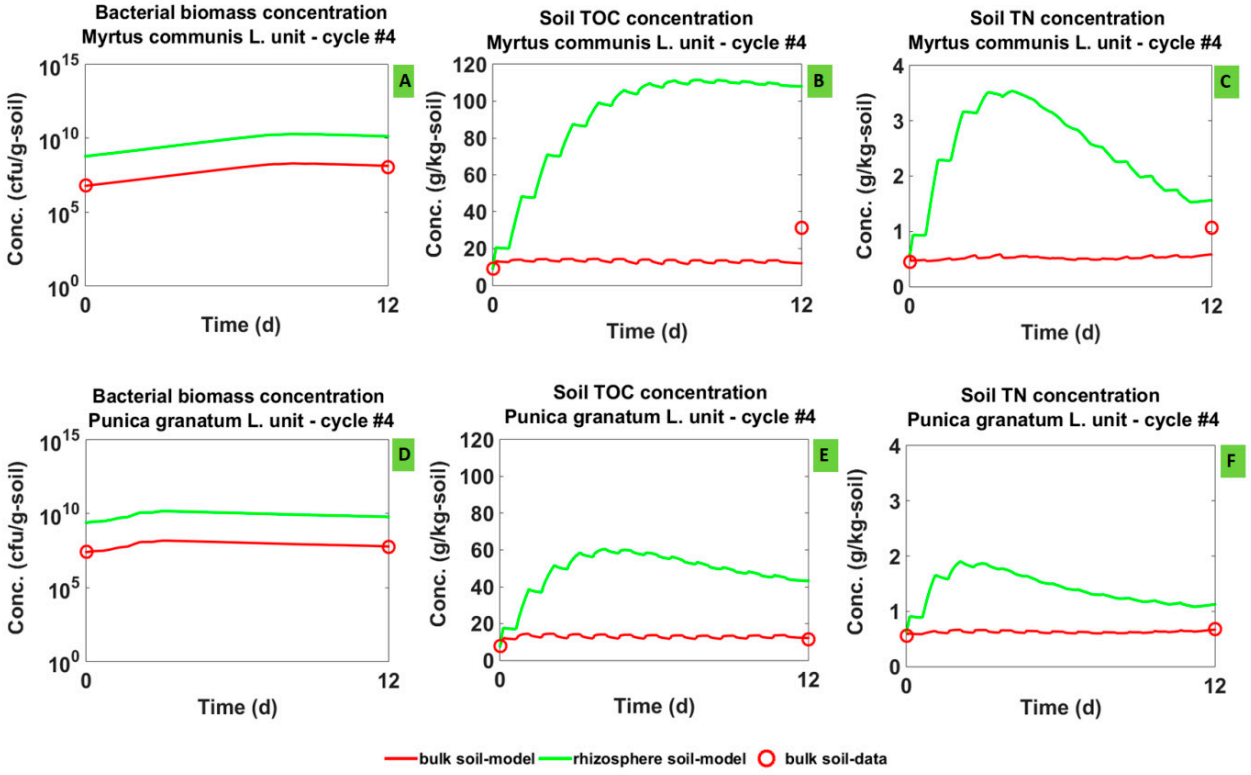

Figure 3. Dynamics of the bacterial biomass, TOC, and TN concentrations of the soil in (**A**–**C**) *P. granatum* and (**D**–**F**) *M. communis* plants units during Cycle #4 (2nd year) of the experiment.

Soil TOC and TN concentrations (Figure 3B,C,E,F) acquire and maintain higher values in the rhizosphere soil (which computationally include the accumulated recalcitrant organics on plants' roots) as compared with the bulk soil in both pilots. Specifically in the case of the *M. communis* plants pilot, the rhizosphere soil acquires disproportionally high TOC and TN concentrations (Figure 3B,C), likely due to the root distribution considered for *M. communis* plants, where the highest proportion of the roots' biomass (79%) is considered to be developed in the top soil compartment.

Experimentally defined values of TOC and TN concentrations for the four soil compartments are not significantly different in any pilot unit, as determined by Petoussi and Kalogerakis (2022) [4]. In addition, there is no certainty that the soil samples were taken from the bulk soil excluding rhizosphere soil. Therefore, the model prediction is satisfactory even in the *M. communis* case since data points of TOC and TN concentrations at the end of the cycle lie between the predicted concentrations of rhizosphere and bulk soil (Figure 3B,C).

3.1.2. Parameter Estimation

Using the LJ optimization procedure, we arrived at the estimated parameter values for the two experimental units shown in Table A4 of Appendix A.6.

Kinetics of Microbial Growth

Maximum specific microbial growth rates for bacteria and fungi ($\mu_{max,b}$ and $\mu_{max,f}$) were estimated by the model in the narrow range of 0.164–0.236 1/h for both pilots. The exception of $\mu_{max,b}$ for the *M. communis* unit estimated as 0.027 1/h (one order of magnitude lower) was examined in the sensitivity analysis. Corresponding specific growth rates reported in studies of OMW degradation kinetics in bioreactors are generally up to two orders of magnitude lower both for bacteria [9,15,17,66] and fungi [5,15,40,67,68], irrespective of the kinetics model used. This inconsistency could result from the fact that in

the model developed in this study, multiple substrate limitation was considered, which required higher maximum growth rates.

Semi-saturation constants for the microbial growth on non-phenolic substrate $K_{S,R,NPh,b}$ and $K_{S,R,NPh,f}$ take values in the range of 32.26–101.19 mg/L, which is lower than the corresponding range of 232–860 mg/L reported by Chiavola et al. (2014) [9], who modeled the kinetics of raw OMW aerobic treatment by activated sludge biomass according to the Monod model. Much higher semi-saturation constants in the range of 4000–18,000 mg/L have also been reported [40,68] for the Monod kinetics growth of fungi on raw OMW. For the microbial growth on low MW phenolics, the semi-saturation constants $K_{S,R,Ph,b}$ and $K_{S,R,Ph,f}$ are in the range of 56.63–82.01mg/L, and inhibition constants $K_{S_i,R,Ph,b}$ and $K_{S_i,R,Ph,f}$ are in the range of 23.12–129.87 mg/L. Similar values of the previous constants were also reported by Tziotzios et al. (2008) [66],who modeled phenol removal by olive pulp bacteria growing in a batch culture following Haldane growth kinetics. The inhibition constants estimated in our model are remarkably low, which gives evidence of the inhibitory action of the phenolic organic substrate [66].

Kinetics of Organic Enzymatic Degradation

Specific rates $k_{dec,\ S,NPh}$ for the decomposition of SBOM are in the range of 10.75–72.73 mg-substrate/g-biomass·h both for bacteria and fungi. Corresponding rates for high MW phenols decomposition $k_{dec,HPh}$ are in the range of 1.02–18.25 mg-substrate/g-biomass·h. The most relevant literature for the decomposition of organic matter in the soil concerns studies in composting of organic wastes, where organic decomposition has been generally modeled as a first-order kinetics process. Corresponding kinetic constants reported for the composting of OMW [16], urban organic waste [69], and specialized organic pollutants, such as PAH, surfactants, and herbicides [70], are more than three orders of magnitude smaller than the estimated kinetic values of our model. The high kinetic constants of this study likely counterbalance the surface limitation considered for the enzymatic decomposition.

Kinetics of Phytoremediation Processes

The estimated value of the transpiration stream concentration factor for the non-phenolic organics $TSCF_{R,NPh}$ equals 1 for both units, resulting from the imposed constraint on the maximum theoretical value of TSCF for the passive plant uptake along with the water used for transpiration. Experimentally defined values of TSCF greater than unity have already been reported in the literature [71]; however, they are not considered to be data of high significance [72]. Values of TSCF for low MW phenols are also greater than 0.95. It was expected that TSCF values would be different for the two plants since uptake efficiency has been reported to vary with plant species, age, and health among others [72,73]. TSCF values derived from the model calibration cannot be directly compared with the corresponding values of the various chemicals reported in the literature [71] since OMW is a mixture of many substances, and TSCF in this case refers to a class of constituents and not to one chemical substance. In addition, large variations have been observed in the literature for compounds with more than one average TSCF, which was attributed to the different experimental approaches and operational variables [74]. TSCF values of inorganic fractions of in-N and P are several times greater than unity, with the exception of the very low phosphorus TSCF value (0.02) for *P. granatum* plants (examined in the sensitivity analysis in Section 3.4). The TSCF value can be greater than unity for nutrients such as nitrogen and phosphorus if they are actively taken up by the plants [75]. Values of TSCF for inorganic nutrients are not available in the literature.

Root concentration factor (RCF) values for the recalcitrant OMW organics (non-phenolic SBOM, high MW phenols, and org-N) in the two units are within the range of the reported values in the relevant literature [76]. Namiki et al. (2018) [77] discussed the different abilities among plant species to take up organic chemicals from the soil into their roots, and they reported RCFs of organic chemicals taking a high range of values.

3.2. Model Validation

As shown in Figure 4, the model predicts very well the dataset of COD (Figure 4C,G) and TPh concentrations (Figure 4D,H) during Cycle#3 for both pilot units (average NRMSE equals 27% and 31% for COD and TPh, correspondingly).

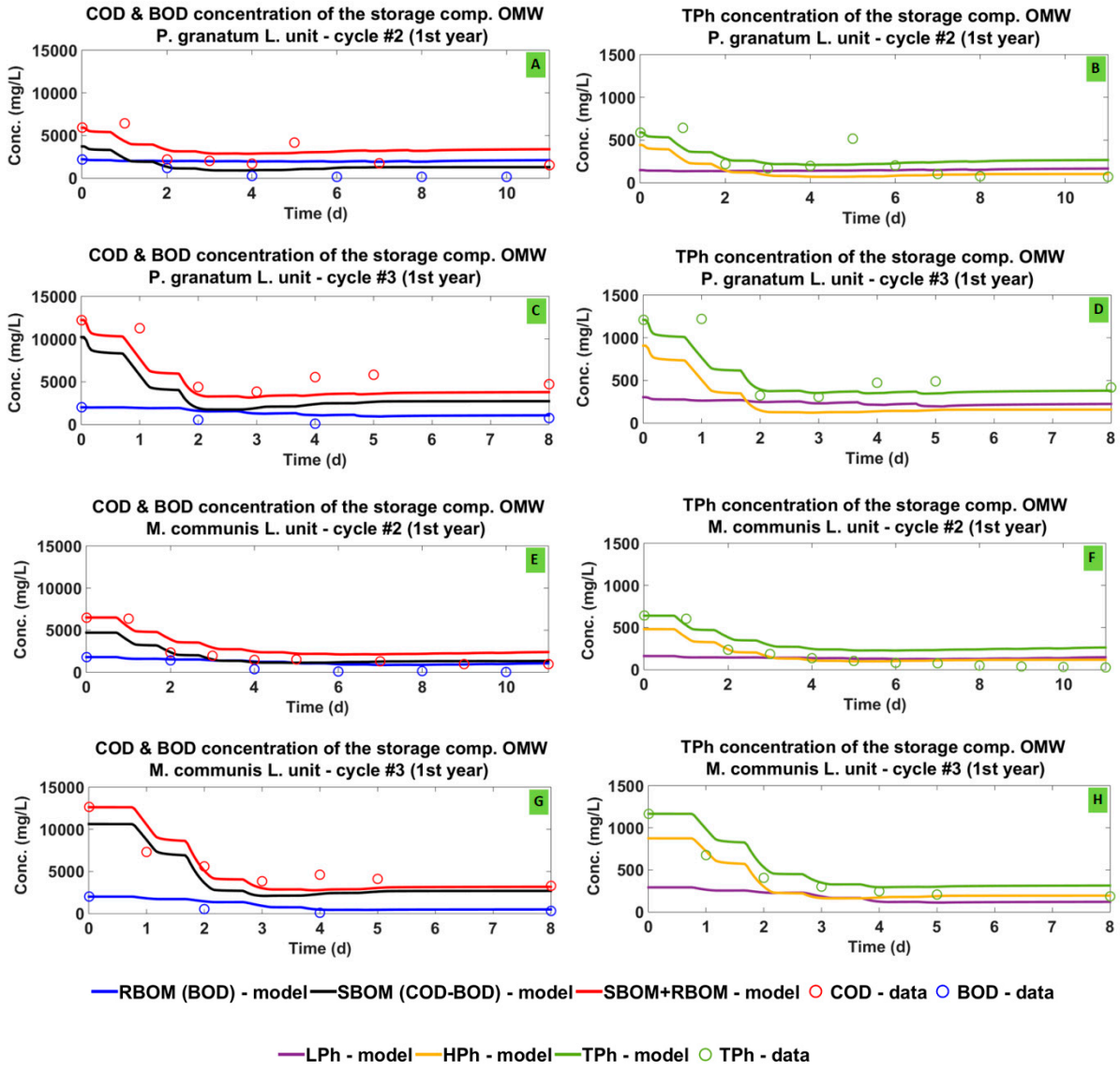

Figure 4. Dynamics of COD, BOD_5,and TPh concentrations of OMW in the storage compartment of (**A**–**D**) *P. granatum* and (**E**–**H**) *M. communis* plants units during Cycles #2 and #3 of the experiment.

During Cycle #2, there is an adequate agreement of the COD (Figure 4A,E) as well as the TPh (Figure 4B,F)concentration data with the model prediction, albeit only until the first half of the cycle. After the 6th day, a positive bias in the prediction of the model is present in both pilots. TN (Figure S5) and TP (Figure S6) concentration data are, however, predicted accurately for Cycles #2 and #3 for both plant units at all time instances, with the exception of TP prediction during Cycle #3, where the data present high fluctuation which cannot be predicted by the model (Figure S6b,d).

Soil TOC, TN, and bacterial biomass concentrations, as shown in Figure 5 for the entire experimental period of the 1st year (Cycles #1–#3),are increasing at the onset of each OMW treatment cycle, as fresh OMW is applied to the soil (time instants t = 0 d, t = 15 d, and t = 27 d).

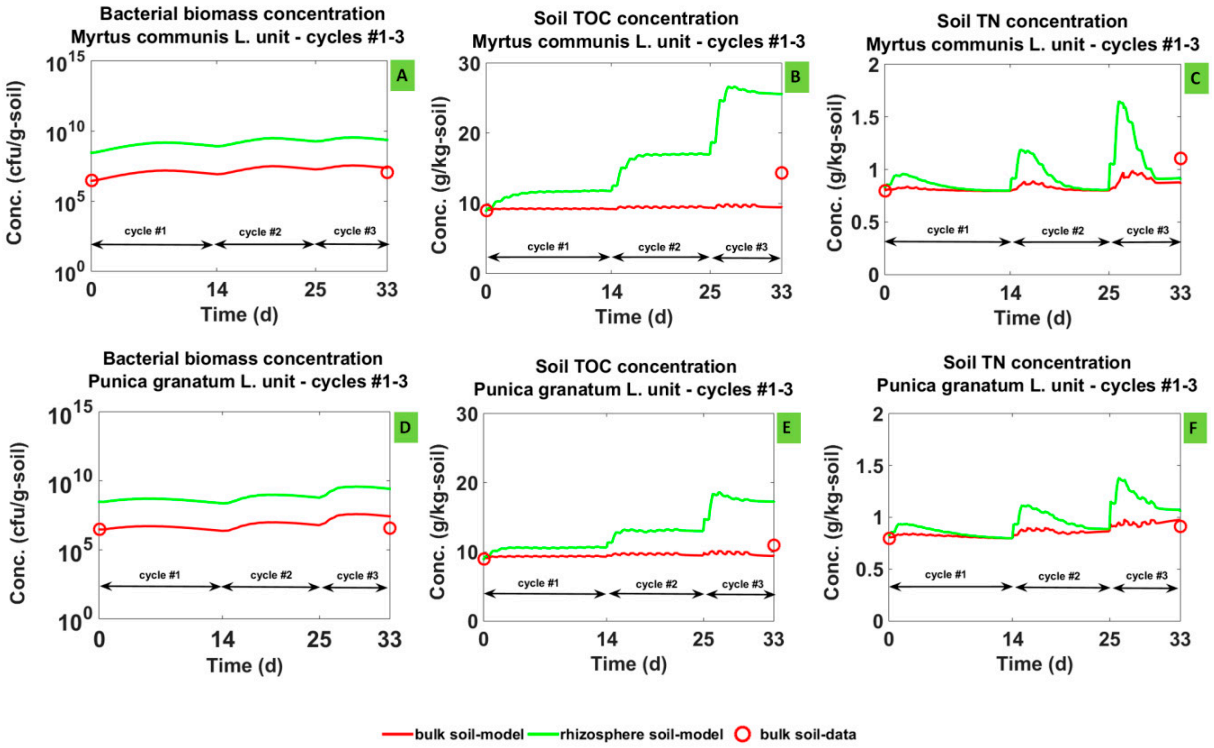

Figure 5. Dynamics of the bacterial biomass, TOC, and TN concentrations of the soil in (**A**–**C**) *P. granatum* and (**D**–**F**) *M. communis* plants units during Cycles #1–3 (1st year) of the experiment.

The bacterial growth rate is proportional to the organic load of the wastewater, as is also referenced by Magdich et al., (2013) [78] and Mekki et al. (2018) [79].The model prediction is satisfactory since data points lie between the predicted concentration of rhizosphere and bulk soil, with the exception of the TN prediction at the end of the experimental year in the *M. communis* unit, which has a relatively low NRMSE of 21%.

3.3. Contribution of the Phytoremediation Processes in the Removal of OMW Organics

Figure 6 shows the relative contribution of the various removal pathways for organics and TPh in the *M. communis* and *P. granatum* pilot units.

Organic removal pathways considered in the model are (a) removal through plant uptake and (b) removal through microbial growth and maintenance in rhizosphere and bulk soil. Mass not removed from the system refers to the total organic mass distributed in the system, e.g., sorbed on the soil, dissolved in the soil solution, concentrated on the plants' roots, or dissolved in the stored wastewater. Corresponding results for TN and TP removal are provided as Supplementary Materials (Figure S7).

As shown in Figure 6, the main organic removal pathway for both units during Cycle #1 is plant evapotranspiration (26–33% COD removal and 18–22% TPh removal). However, during the next cycles (#2 and #3), plant evapotranspiration contributes less to organic removal, whereas consumption by rhizosphere microbial biomass gradually increases its contribution up to 5–8% COD and 4–10% TPh removal at the end of Cycle #3, where more bioavailable organic substrate and nutrients are present in the wastewater, thus promoting microbial growth. At Cycle #3, plant evapotranspiration and consumption by rhizosphere microbial biomass contribute almost evenly to organic removal and together by 11–13% COD removal and 12–18% TPh removal. Plant evapotranspiration is the main pathway for organic removal at Cycle #4, corresponding to 25–29% COD and 12–15% TPh removal, which could be attributed to the higher evapotranspiration rate of plants during the 2nd experimental year.

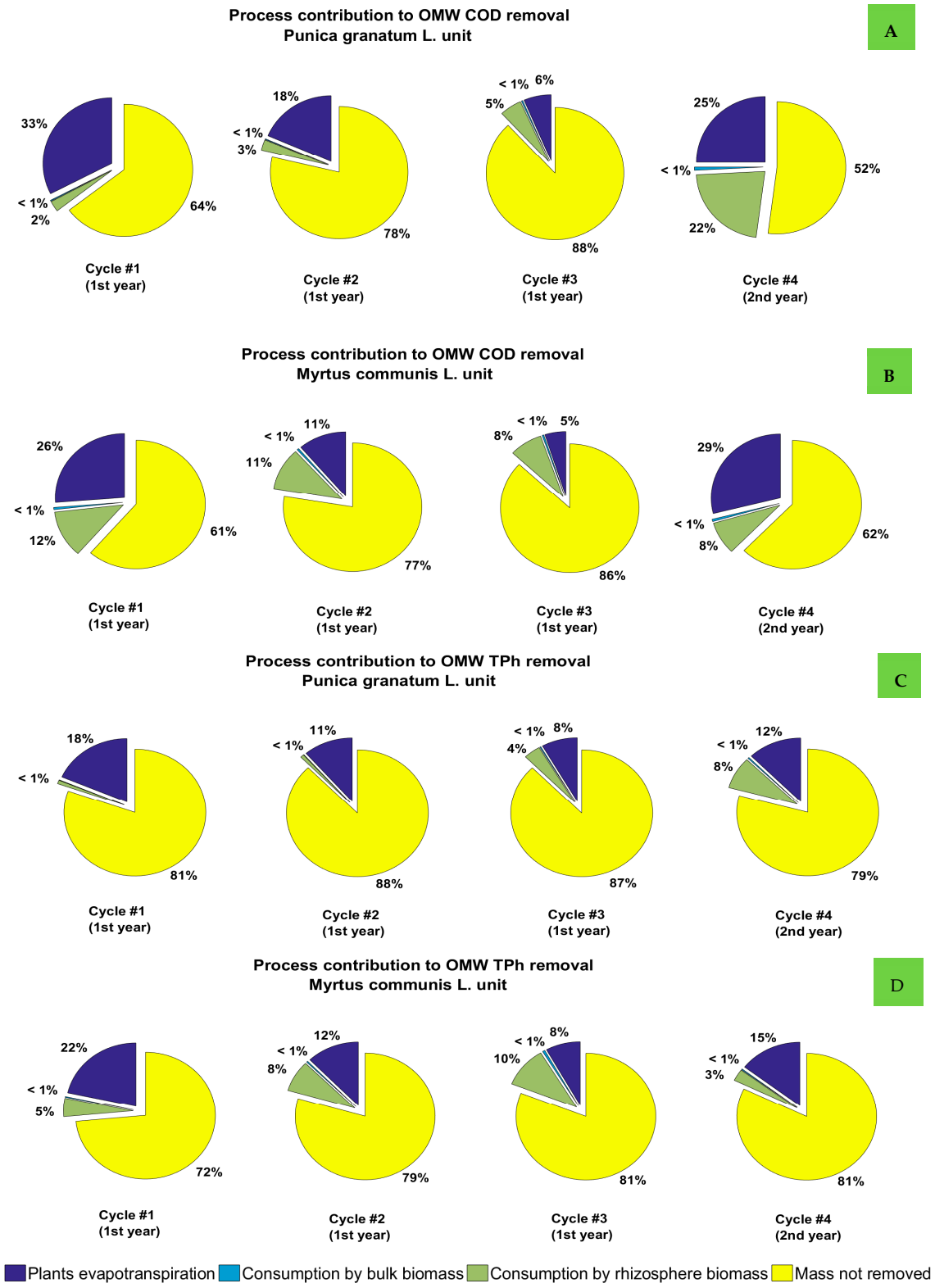

Figure 6. Percentage contribution of the various processes for (**A**,**B**) COD and (**C**,**D**) TPh mass removal in *P. granatum* and *M. communis* units for all experimental cycles.

TN (Figure S7a,b) is removed mainly through plants uptake and by more than 79% and 61% in *M. communis* and *P. granatum* pilots, respectively, in all cycles of the first year. Computationally, this performance is in line with the active uptake of inorganic nitrogen by plants and in accordance with the corresponding TSCF values greater than unity (Table A4).

However, at Cycle #4, consumption by rhizosphere microbial biomass is also contributing highly to TN removal by 50% and 20% of the total wastewater TN mass for the *P. granatum* and *M. communis* units, respectively. It is noted that denitrification was neglected in the model for the purpose of simplification, as it contributed less than 1% in the removal of TN.

In the case of TP (Figure S7c,d), there is a difference between the two pilots regarding the main removal TP pathway, i.e., in the *P. granatum* unit, phosphorus is precipitated mainly in all cycles (>86% in 1st year's cycles and 61% in Cycle #4), whereas in the *M. communis* unit, it is also taken up by plants in a high percentage (27–40% in 1st year's cycles and 45% in Cycle #4 of the 2nd year). This is computationally attributed to the large discrepancy between the TSCF values for TP in the two units ($TSCF_P$ equal to 0.02 and 2.83 for the *P. granatum* and *M. communis* units, correspondingly) since precipitation constant values k_{prec} are similar for the two pilots.

The contribution of the bulk soil microbial biomass activity to the removal of all wastewater compounds is minimal (less than 1%) in all cycles for both units, and more specifically, it does not exceed 9% of the total removed organic amount in any of the cases. Overall, this indicates that the phytoremediation processes (plant uptake and rhizodegradation) contribute in all cases by more than 91% to the organic removal in the context of the present study. It is noted, however, that removal percentages should not be compared among experimental cycles, as they refer to different initial wastewater concentrations, i.e., the decreasing trend of the removal of organics from Cycle #1 to Cycle #3 is not indicative of a less effective system.

It is also noted that the mass of the removed organics (COD and TPh) from the pilot system estimated by the model is, in all cases, substantially lower than the one evaluated by Petoussi and Kalogerakis (2022) [4] since the model considers accumulation on the plants' root tissue in addition to adsorption on soil.

3.4. Sensitivity Analysis

A sensitivity analysis of the model was performed according to the procedure outlined by Zhang et al. (2012) [69]. Each model parameter was increased independently by 5% from its estimated value. The sum of the deviation of all SVs considered for the wastewater in the storage compartment and SVs of microbial biomass concentration at specific time instances of each of the four experimental cycles were considered as the sensitivity coefficient σ (Equation (30)).

$$\sigma(P) = \frac{1}{N_{cycles}} \sum_{cycle=1}^{N_{cycles}} \frac{1}{N_{sv}} \sum_{SV=1}^{N_{sv}} \frac{1}{N_f} \sum_{0}^{N_f} \left| \frac{SV(P_0 + 5\%, t) - SV(P_0, t)}{\overline{SV(P_0)}} \right| \quad t = 0,\ 1,\ 2, \ldots,\ N_f \tag{30}$$

where N_{cycles} is the number of experimental cycles (4), N_{sv} is the number of *SVs* considered for the sensitivity analysis, $SV(P_0, t)$ is the value of the state variable SV at time t when parameter P has its calibrated value P_0, $SV(P_0 + 5\%, t)$ is the value of the state variable SV at time instant t when parameter P has its calibrated value Po increased by 5%, and $\overline{SV(P_0)}$ is the mean value of the SV. The sensitivity coefficients of all estimated model parameters are presented in Table A5 of Appendix A.6 for both pilot units.

Parameters with sensitivity coefficient $\sigma > 0.01$ were further assessed for their impact on the system's removal efficiency for COD and TPh based on the simulation of Cycle #4 (with high-organic-strength wastewater). In this context, each parameter was increased by a certain percentage, and the normalized percent variation in the removal of COD and TPh by each process was assessed. A few additional model inputs related to the plants and wastewater characteristics were also investigated. Results are provided in Table A6 of Appendix A.6. As shown, the estimated parameters causing the greatest percent variation in COD and TPh removal (with absolute coefficients greater than 0.3) are related to nutrients availability and maximum microbial biomass growth specific rates and, therefore, have an impact on organic removal through microbial consumption (biomass growth and maintenance). Among those parameters, k_{prec} and $\mu_{max,f}$ have the

greatest impact on the removal of COD and TPh for the *P. granatum* and *M. communis* units, respectively. However, for a 20% increase in those parameters, an increase in COD and TPh removal does not exceed 8% and 25%, correspondingly, for the two pilot units, which, in both cases, provides no more than 1.5% additional removal.

Among the parameters related to the wastewater synthesis, the percentage of high MW polyphenols to total polyphenols $\left(\frac{C_{HPh}}{C_{HPh}+C_{LPh}}\right)_0$ affects strongly affects TPh removal through both microbial consumption and plant evapotranspiration in both units. This is expected, due to the change of the low MW phenols availability for the previous processes. A 20% increase in high MW polyphenols leads to a reduction in TPh removal up to 57% through plant uptake and up to 47% through rhizosphere microbial biomass activity in both units.

In addition, important variation in organic removal is also caused by the parameter m_{tissue} related to the root system of the plants, which is expected since it causes variation in the concentration of organics on the plants' roots. A 20% increase in m_{tissue} parameter leads to a 9% and 14.5% reduction in COD and TPh removal, correspondingly.

Concerning the kinetic parameters which are estimated with very diverse values for the two pilot units (Table A4), the sensitivity analysis shows that $\mu_{max,b}$, $TSCF_P$, and $k_{S,in-N,f}$ are more sensitive in the *M. communis* pilot system, and $k_{S,P,f}$ and $K_{S,in-N,b}$ are more sensitive in the *P. granatum* system; thus, the estimated values for the corresponding systems are considered to be more reliable.

Generally, according to the sensitivity analysis results, the removal efficiency of the system is expected to be improved in the case of an extra supply of nutrients N and P in a soil environment where the growth of fungi species is promoted. For higher efficiency of the system in TPh removal, treatment of the wastewater soon after its production should be considered in order to maintain a lower fraction of high MW polyphenols.

The developed model is macroscopic and is based on available experimental data [4]. Therefore, it has some limitations, among which the most important are: (a) the effect of OMW pH and temperature on the rates of the microbial processes was taken into account, (b) the modeling of highly computationally demanding diffusion processes, as well as the consideration of additional soil compartments for the rhizosphere zone, were excluded, which could affect the availability of OMW solutes for both microbial consumption and removal by plants through transpiration, (c) the model calibration was not based on the soil fungal concentration (due to lack of experimental data), which could underestimate the role of the corresponding microbial population in OMW treatment, (d) the accumulated recalcitrant organics on the plants' roots were not considered to be degraded in the interest of model simplification, which is not very realistic since they are degraded by the rhizosphere microbial biomass, and (e) the values of the roots' tissue mass of the plants m_{tissue} as well as the OMW initial high MW polyphenols fraction $\left(\frac{C_{HPh}}{C_{HPh}+C_{LPh}}\right)_0$ were based on the relevant literature data (due to lack of experimental data).

4. Conclusions

An integrated macroscopic mechanistic model was developed to describe the dynamics of OMW degradation during its short-term recirculation in the soil of two phytoremediation pilot units using plants of the *P. granatum* L. and *M. communis* L. species. An innovation of the model is the discretization of the total labile organic substrate of OMW to a phenolic and a non-phenolic fraction, consumed by both bacteria and fungi. The model effectively predicted the experimental data from the treatment of medium- and high-organic-strength wastewater. The maximum specific kinetic rates of microbial growth and organics decomposition were evaluated through the model calibration process to be more than two orders of magnitude higher than the corresponding rates reported in studies of OMW degradation in bioreactors or in studies of composting processes for various organics. The values of TSCF for the non-phenolic and phenolic fractions of OMW organics were estimated as greater than 0.95, which indicate almost passive uptake of the OMW organic mixture by

the plants. TSCF factors of inorganic N and P have been estimated as greater than unity, indicating corresponding active uptake of these ingredients.

The relative contribution of plant uptake and rhizodegradation processes in the OMW organic removal varies among the treatment cycles since it depends on both the evapotranspiration rate of plants and the microbial biomass concentration in their rhizosphere. However, the total contribution of both processes on the overall treatment of OMW was specified as more than 91% during treatment of low- or high-organic-strength OMW in both pilot units.

The estimated kinetic parameters causing the greatest percent variation in organic removal are related to the nutrients availability in the system and the microbial maximum specific growth rates, as investigated through the sensitivity analysis of the model. However, for a 20% increase in those parameters, the additional absolute removal of OMW organics mass did not exceed 1.5%. The most important parameter for the removal of polyphenols was the percentage of high MW polyphenols concentration over the total polyphenols concentration. An increase in the previous parameter caused a substantial decrease in polyphenols removal from the system.

Generally, according to the sensitivity analysis results, the efficiency of the system is expected to be improved in the case of an extra supply of nutrients N and P to the system and promotion of the fungal growth. For higher efficiency of the system in TPh removal, treatment of the wastewater soon after its production should be considered in order to maintain a lower fraction of high MW polyphenols.

Supplementary Materials: The following supporting information can be downloaded at: https://www.mdpi.com/article/10.3390/su15118630/s1. The following supporting information is available: Figures S1–S9.

Author Contributions: Conceptualization, N.K. and M.A.P.; methodology, M.A.P.; software, M.A.P.; validation, M.A.P.; formal analysis, N.K. and M.A.P.; data curation, M.A.P.; writing—original draft preparation, M.A.P.; writing—review and editing, N.K.; supervision, N.K.; funding acquisition, N.K. All authors have read and agreed to the published version of the manuscript.

Funding: Financial support by the project "INVALOR: Research Infrastructure for Waste Valorization and Sustainable Management" (MIS 5002495), which is implemented under the Action "Reinforcement of the Research and Innovation Infrastructure", funded by the Operational Programme "Competitiveness, Entrepreneurship and Innovation"(NSRF 2014–2020) and co-financed by Greece and the European Union (European Regional Development Fund) is greatly appreciated.

Institutional Review Board Statement: Not applicable.

Informed Consent Statement: Not applicable.

Data Availability Statement: Data are available upon request.

Conflicts of Interest: The funders had no role in the design of the study; in the collection, analyses, or interpretation of data; in the writing of the manuscript; or in the decision to publish the results.

Appendix A

Appendix A.1. Plants' Root Biomass and Distribution in the Unit

Due to lack of experimental assessment of the plants' root system characteristics in the pilots, we based our assumptions concerning their roots' tissue mass and distribution on the most relevant available information found in the literature. More specifically, assumptions for the root system of the pomegranate trees were based on the work of Marathe et al. (2017) [63], who studied the root distribution in terms of root mass and root length in four-year-old trees of pomegranate cv. Bhagwa grown in light textured, shallow soil type. We adopted the same mass of root tissue per tree and the same distribution pattern in the upper 30 cm of the phytoremediation unit. Accordingly, for the myrtle trees, our assumptions were based on the study by Silva et al. (2003) [80], who modeled the relative cumulative root biomass distribution and root length as a function of depth for *M. communis*

plants. The root distribution incorporated in the model for the myrtle plants was derived from the implementation of the proposed model for *M. communis* species at a maximum depth of 40 cm soil layer. For the plants' root tissue, since there were no relevant data in the literature, we adopted the same value as in *P. granatum* trees and included this parameter in the sensitivity analysis of the model. During the second year's experimental cycle, root tissue mass m_{tissue} (kg-root tissue/tree) was considered double for both plant units; however, the root distribution remains b remained the same as during the first experimental year.

Appendix A.2. Wastewater Flow through the Unit

Wastewater's gravitational flow through the soil of the unit was considered to be one-dimensional. Due to the intermittent irrigation of the unit, the wastewater flow was expected to take place both under saturated and unsaturated conditions and was considered to follow a combination of the Darcy–Buckingham model and the "tipping bucket" approach [19,20]. More specifically, the vertical flux density q (m/d) in a uniformly wet soil is described by

$$q(\theta_v) = K(\theta_v) \quad \text{(A1)}$$

where K is the soil hydraulic conductivity (m/d), which is a function of the volumetric soil water content θ_v (m^3/m^3) [81]. Kendy et al. (2003) [82] suggested that $K(\theta_v)$ can be expressed by the exponential relationship:

$$K(\theta_v) = K_{sat} exp\left(-\alpha \frac{\theta_{v,sat} - \theta_v}{\theta_{v,sat} - \theta_{v,r}}\right) \quad \text{(A2)}$$

where K_{sat} is the saturated hydraulic conductivity, α is an empirical coefficient (dimensionless), and $\theta_{v,sat}$ and $\theta_{v,r}$ are the saturated and residual volumetric soil water content, respectively. Water infiltration through the soil in transient conditions can lead to water accumulation in a layer up to a point (maximum water holding capacity), where excess water must percolate into successively lower layers ("tipping bucket" scheme). It should also be noted that during infiltration, water is considered to be lost through evaporation (only from the top soil compartment) and the plants' evapotranspiration (corresponding rates are provided in Table A3). Therefore, the wastewater volume balance in the kth soil compartment of the unit can be described by Equation (A3):

$$\frac{dV_k}{dt} = \begin{cases} Q_{pump} - Q_k - q_{ET,k} - q_{EV} - Q_{e,k}, & k = 1 \\ Q_{k-1} - Q_k - q_{ET,k} - Q_{e,k}, & k = 2,3,4 \end{cases} \quad \text{(A3)}$$

where Q_{pump} is the wastewater pumping rate, $Q_k = AK(\theta_{v,k})$ is the output flow rate from the kth layer due to the wastewater redistribution over the cross sectional area A (m^2), $q_{ET,k}$ is the plants' transpiration rate in the kth layer, q_{EV} is the evaporation rate from the top layer of the unit, and $Q_{e,k}$ is the wastewater percolation rate from the kth layer in the case of excess of water.

Appendix A.3. Wastewater Volume Loss through Evaporation and Plant Evapotranspiration

The total volume of the wastewater in the system was considered to be gradually reduced through both water evaporation and the plants' evapotranspiration. Thornthwaite's formula was incorporated in the model to account roughly for the daily potential evaporation based only on temperature data [83]. Due to the long-lasting and high flow rate application of the wastewater during the daytime, actual daily evaporation was assumed to equal the potential evaporation. Meteorological data for the entire experimental period were provided from the meteorological station of the Technical University of Crete, located near the experimental units' settlement.

Water uptake by plants is generally a function of time and soil depth, and many empirical mathematical formulations have been developed to describe its rate on the basis

of soil matric suction, considered favored for simulation models [84].We herein adopted the often used Feddes–Jarvis model [85], described briefly below:

First, the potential root water uptake rate $S_p(1/s)$ was calculated, as determined by the potential transpiration rate T_p(cm/s) and the normalized root length density distribution $b(z)$ (1/cm),

$$S_p(z,t) \;=\; b(z)T_p(t) \tag{A4}$$

The potential uptake rate was then converted into the reduced uptake rate $S(1/s)$ by multiplying S_p with by the dimensionless stress reduction factor $a_r(z,t)$ accounting for stress due to oxygen deficit and matric suction ($0 \le a_r \le 1$),

$$S(z,t) \;=\; a_r(z,t)S_p(z,t) \tag{A5}$$

Factor a_r is often described by a piecewise linear reduction function, parameterized by four critical values of the matric suction, $\psi_4 < \psi_3 < \psi_2 < \psi_1$:

$$a_r(\psi) \;=\; \begin{cases} 0, & \psi \ge \psi_1 \\ \dfrac{\psi_1 - \psi}{\psi_1 - \psi_2}, & \psi_1 > \psi \ge \psi_2 \\ 1, & \psi_2 > \psi \ge \psi_3 \\ \dfrac{\psi - \psi_4}{\psi_3 - \psi_4}, & \psi_3 > \psi \ge \psi_4 \\ 0, & \psi_4 \ge \psi \end{cases} \tag{A6}$$

The values of ψ_2 and ψ_3 represent the thresholds between which water uptake is assumed to be maximum, while ψ_1 and ψ_4 represent, respectively, the thresholds of oxygen deficiency due to soil saturation and the minimum soil water content observed in the core of the root system (generally close to the wilting point).

Matric suction ψ of the unit's soil at each soil's water content was calculated by the soil characteristic curve for sandy soils provided by Fredlund and Xing (1994) [86]. Total wastewater volume loss due to plants evapotranspiration plus evaporation was considered to follow the experimentally estimated daily wastewater volume reduction rate from the storage compartment. Total daily transpired water volume through plant roots $V_{tot,transp}(t)$ (L/h)was computationally distributed to the four soil compartments according to the weighted function of Equation (A7), taking into account both the plants' root distribution b_k and the water stress factor $a_r(k,t)$ in each layer:

$$q_{ET,k}(t) \;=\; S(k,t) \;=\; \left(b_k a_r(k,t) / \textstyle\sum_j \left(b_j a_r(j,t)\right)\right) V_{tot,transp} \tag{A7}$$

where $S(k,t)$(L/h) is the transpired water volume in the kth layer at time t, b_k is the percentage of root biomass at the kth layer, and $a_r(k,t)$ is the stress factor at the kth layer at time t. Nocturnal root water uptake was considered to be zero, as in most soil–plant–atmosphere continuum models [84]; thus, plants evapotranspiration was considered to take place during the daytime (12 h/d) while the wastewater pump was also in operation.

Appendix A.4. Solutes Transport and Distribution in the Soil

Solutes were considered in the system to be distributed between the solid phase (soil) and the liquid phase (soil solution). Adsorption of OMW constituents on the soil was modeled by the linear type adsorption isotherm.

Adsorption and desorption are considered to be instantaneous processes, i.e., thermodynamic equilibrium between liquid and soil phase was considered at all time instants. Partition coefficients K_{sd} for the total organic, polyphenolic, nitrogenous, and phosphorus compounds were given by Petoussi and Kalogerakis (2022) [4]. Since microbial biomass is considered to take up constituents only from the soil solution, adsorption on soil had

a storage-like role in the model, whereby adsorbed compounds entered the soil solution gradually while the wastewater was remediated.

Microbial biomass is generally distributed on the inner surface of the soil pores, forming a biofilm. As in most macroscopic biodegradation models [87], we herein adopted the common approach of "no diffusion resistance" of biofilm, i.e., the effect of microscale biofilm phenomena was lumped into the estimated overall degradation rates. Moreover, a constant surface-to-volume ratio was considered for the biofilm, and the microbial biomass concentration in the model was expressed in terms of soil mass.

Mass diffusion in the aqueous phase of the soil was reported to be considerably affected by the soil's water content θ_v, which is the most important parameter influencing effective diffusion coefficient D_e in unsaturated soils [88].Therefore, in order to account for the effect of the soil's water content on the diffusion of soluble OMW substrates and their availability to microbial biomass, a simplistic approach was followed in the model to avoid high computational complexity. We considered, therefore, each substrate's concentration in the interface between the biofilm and the bulk soil solution C_{int} to be proportional to the corresponding diffusion coefficient D_e according to the current water content, following Equation (A8):

$$C_{int}/C_{bulk} = D_e/D_o \quad \text{(A8)}$$

where C_{bulk} denotes the substrate's concentration in the bulk soil solution.

We herein adopted the empirical expression of Millington and Quirk (MQ) [89], where D_e of a solute in a soil system can be estimated from the solute's diffusion coefficient in water D_o (m^2/s), soil porosity, and soil water content by Equation (A9):

$$D_e = D_o\left(\theta_v{}^{\frac{7}{3}}/\theta_{v,sat}{}^2\right) \quad \text{(A9)}$$

where $\theta_{v,sat}$ (m^3/m^3) is the total porosity of the soil, and θ_v (m^3/m^3) is the current water content of the soil. At the wilting point, C_{int} = 0 mg/L.

Appendix A.5. Olive Mill Wastewater Oxygenation

Since OMW is not aerated while being in the storage compartment, and its initial dissolved oxygen (DO) content is not sufficient to sustain microbial growth during the whole experimental period, it is deduced that the wastewater is oxygenated while being in contact with the atmospheric air at the surface of the unit during drip irrigation and also while being in contact with the air of soil pores (in unsaturated conditions) during wastewater infiltration through the soil. Whenever the soil pores become waterlogged at high volumetric flow rates, no wastewater oxygenation takes place. Note that the soil layer of the two units, due to its relatively small depth (45 cm) and its sandy texture, is assumed to be well aerated during the drainage period after the daily pump shut-off due to the siphoning effect [7]. Moreover, the plants' roots may improve the diffusion of oxygen to deeper soil layers by providing channels for air flow as they decay or desiccate or by decreasing the soil bulk density. Maximum DO concentration of the OMW was calculated by the equations of Garcia and Gordon (1992) [90], with parameters given by Benson and Krause (1984) [91]. Although the former equations are valid for calculating oxygen solubility in seawater, they were used herein as the best available reference to calculate the possible maximum DO concentration of the OMW. Salinity and temperature data required by the equations were assumed to match the wastewater salinity and air temperature (due to lack of wastewater temperature data). Moreover, since there was likely not enough contact time for oxygen diffusion between the soil air pockets and the wastewater in order to reach equilibrium, it was assumed that DO concentration of OMW corresponded to only 50% of the maximum DO concentration, which was chosen during the model development to match the experimental oxygen concentration profile. The level of OMW oxygenation was also considered in the model sensitivity analysis.

Appendix A.6. Tables

Table A1. Kinetic rates of all processes in the mass balance of each state variable.

State Variable	Plant Uptake (Transpiration)	Adsorption on Plants' Roots *	Enzymatic Decomposition	Ammonification	Biomass Growth	Biomass Decay	Biomass Maintenance	Phosphorus Precipitation
$C_{S,NPh}$		$-/+R_{S,NPh,ads}$	$-R_{S,NPh,dec}$			$+R_{S,NPh,decay}$		
$C_{R,NPh}$	$-R_{R,NPh,uptake}$		$+R_{S,NPh,dec}$		$-R_{R,NPh,growth}$		$-R_{R,NPh,mainten}$	
C_{HPh}		$-/+R_{HPh,ads}$	$-R_{HPh,dec}$					
C_{LPh}	$-R_{LPh,uptake}$		$+R_{HPh,dec}$		$-R_{LPh,growth}$		$-R_{LPh,mainten}$	
C_{org-N}	$-R_{org-N,uptake}$	$-/+R_{org-N,ads}$		$-R_{org-N,ammon}$		$+R_{org-N,decay}$		
C_{in-N}	$-R_{in-N,uptake}$			$+R_{org-N,ammon}$	$-R_{in-N,growth}$			
C_P	$-R_{P,uptake}$				$-R_{P,growth}$			$-R_{P,prec}$
C_O	$-R_{O,uptake}$				$-R_{O,growth}$		$-R_{O,mainten}$	
$X_{b,b}$ and $X_{b,r}$					$+\mu_b X_b$	$-d_b X_b$		
$X_{f,b}$ and $X_{f,r}$					$+\mu_f X_f$	$-d_f X_f$		
$S_{ads,S,NPh}$		$-/+R_{S,NPh,ads}/m_{tissue}$						
$S_{ads,HPh}$		$-/+R_{HPh,ads}/m_{tissue}$						
$S_{ads,\ org-N}$		$-/+R_{org-N,ads}/m_{tissue}$						

* the + or − sign is chosen based on the adsorption potential.

Table A2. List of limitation expressions for microbial growth.

Limitation Type	Expressions
Monod kinetics for non-phenolic RBOM substrate	$\varphi_{Mnd,y} = \frac{C^*_{R,NPh}}{K_{S,R,NPh,y}+C^*_{R,NPh}}$
Haldane kinetics for phenolic RBOM substrate	$\varphi_{Hld,y} = \frac{C^*_{R,Ph}}{K_{S,R,Ph,y}+C^*_{R,Ph}+\frac{{C^*_{R,Ph}}^2}{K_{S_i,R,Ph,y}}}$
Monod kinetics for oxygen	$\varphi_{O,y,aer} = \frac{C^*_O}{K_{S,O,y}+C^*_O}$
Inverse Monod kinetics for oxygen inhibition for bacterial anoxic growth	$\varphi_{O,b,anox} = \frac{K_{S,O,b}}{K_{S,O,b}+C^*_O}$
Monod kinetics for NO_3-N for bacterial anoxic growth	$\varphi_{NO_3,anox} = \frac{\eta_{NO_3}\cdot C^*_{in-N}}{K_{S,NO_3,b}+\eta_{NO_3}\cdot C^*_{in-N}}$
Monod kinetics for inorganic nitrogen	$\varphi_{in-N,y} = \frac{C^*_{in-N}}{K_{S,in-N,y}+C^*_{in-N}}$
Monod kinetics for inorganic phosphorus	$\varphi_{P,y} = \frac{C^*_P}{K_{S,P,y}+C^*_P}$
Fraction of non-phenolic RBOM	$f_{NPh} = \frac{C^*_{R,NPh}}{C^*_{R,NPh}+C^*_{R,Ph}}$
Fraction of phenolic RBOM	$f_{Ph} = \frac{C^*_{R,Ph}}{C^*_{R,NPh}+C^*_{R,Ph}}$

Symbol "*" denotes the states for the solute concentration at the biofilm interface C_{int} (Appendix A.4). $k_{S,i,y}$ (mg/L) denotes semi-saturation constant of constituent i in the growth rate of population y. i denotes the states for non-phenolic RBOM, phenolic RBOM, in-N, P, and oxygen; and y denotes the states for bacteria or fungi; $K_{S_i,R,Ph,y}$ (mg/L) denotes inhibition constant for phenolic RBOM in the growth rate of population y; η_{NO_3} (dimensionless) denotes $NO_3{}^-N$ fraction of in-N.

Table A3. Model input parameters.

	Symbol	Description	Value *	Unit	Source of Parameter Value
Biomass stoichiometric yields	$Y_{X_y/R,NPh}$	Biomass yield per unit substrate consumed	b: 3.94×10^{-4}, f: 6.44×10^{-4}	g-biomass/mg-substrate	Calculated on the basis of biomass chemical formulae by [15]
	$Y_{X_y/N}$		b: 8.3×10^{-3}, f: 17.9×10^{-3}		
	$Y_{X_y/P}$		b: 27.8×10^{-3}, f: 62.5×10^{-3}		
	$Y_{X_y/O}$		b: 3.6×10^{-3}, f: 2.6×10^{-3}		
Conversion factors	$c_{f,b,SBOM}$	Conversion coefficients of decayed microbial biomass to non-phenolic SBOM	$113 \times 10^{-3}/160$	g-biomass/mg-COD	
	$c_{f,f,SBOM}$		$367 \times 10^{-3}/672$	g-biomass/mg-COD	
	$\boldsymbol{c_{f,PhBOD}}$	Equivalent BOD_5 of gallic acid	192 /170	mg-BOD_5/mg-gallic acid	
Biomass processes' kinetic constants	k_m	Biomass maintenance constant	b: 7, f: 7	mg/g-biomass h	[92]
	d	Biomass decay specific rate	b: 5.7×10^{-3}, f: 5.7×10^{-3}	1/h	[93]
	r_d	Fraction of decayed biomass contributing to SBOM pool	0.5	-	[16]
	$k_{S,O}$	Saturation constant for oxygen limitation factor	b: 2×10^{-3}, f: 7×10^{-3}	mg/L	[94]
	k_X	Saturation constant of surface limitation factor	100	(mg-substrate/L)/(g-biomass/kg-soil)	[42]
Assumptions on OMW and soil characteristics	$\left(\frac{C_{HPh}}{C_{HPh}+C_{LPh}}\right)_0$	Initial fraction of high MW polyphenols over TPh	0.75	-	[95]
	$\left(\frac{C_{org-N}}{C_{org-N}+C_{in-N}}\right)_0$	Initial fraction of org-N over TN	0.85	-	[44,81,82,96,97]
	$\frac{C_{NO_3^- -N}}{C_{in-N}} = \eta_{NO_3}$	Fraction of $NO_3{}^-$N over in-N	0.15	-	[44,81,82,96,97]
	$\left(\frac{X_f}{X_b}\right)_0$	Initial fraction of fungal biomass over bacterial biomass	0.3 (both in bulk and rhizosphere soil–1st and 2nd year)	-	[98]
	$\left(\frac{X_{rhizosphere\ biom}}{X_{bulk\ biom}}\right)_0$	Initial fraction of rhizosphere biomass concentration over biomass of bulk soil (both bacteria and fungi)	100	-	[62]
	$\frac{M_{rhizosphere\ soil}}{M_{total\ soil}}$	Fraction of rhizosphere soil over unit's total soil	1st year: 0.1 2nd year: 0.2	-	Calculatedon the basis of [1,63,64]

Table A3. *Cont.*

	Symbol	Description	Value *	Unit	Source of Parameter Value
Solutes Transportation and hydrodynamic-related constants	$K_{sd,i}$	Partition coefficient for constituent i	COD: 0.509; TPh: 0.508; TN: 0.443; TP: 6.199	L/kg-soil	Experimentally determinedby [4]
	K_{sat}	Saturated hydraulic conductivity	15.21	m/d	[81]
	$\theta_{v,r}$	Residual volumetric soil content	0.02	m^3/m^3	[99]
	$\theta_{v,sat}$	Saturated volumetric soil content	0.43	m^3/m^3	[81]
	α	Empirical coefficient	13	-	[81]
	d_{soil}	Soil density	1.14	kg/L	Experimentally determined by [4]
Distribution and biomass of plants roots	m_{tissue}	Total root tissue mass of plants	*P. granatum*: 0.9927 *M. communis*: 0.9927	kg/tree	Calculatedon the basis of [63]
	b_k	Percentage of root tissue massat the *k*th layer	*P. granatum*: b_1 = 22.96; b_2 = 24.77; b_3 = 25.50; b_4 = 26.77 *M. communis* L.: b_1 = 78.73; b_2 = 9.47; b_3 = 5.59; b_4 = 6.21	%	Calculatedon the basis of [1,63,80]
	ψ_k	Matric potential thresholds of Feddes piecewise linear reduction function	$\psi_1 = 0$ $\psi_2 = -25$ $\psi_3 = -400$ $\psi_4 = -8000$	cm	ψ_1, ψ_2, and ψ_4 [7,85,100], ψ_3 [7,85,100–103]

* symbols *b* and *f* refer, correspondingly, to bacteria and fungi.

Table A4. Values of the calibrated parameters of the model.

Related Process	Parameter	Unit	Pilot Unit	
			P. granatum	*M. communis*
Plant uptake	$TSCF_{R,NPh}$	-	1.00	1.00
	$TSCF_{LPh}$		0.95	1.00
	$TSCF_{in-N}$		7.02	11.80
	$TSCF_{org-N}$		0.67	0.29
	$TSCF_{P}$		0.02	2.83
Adsorption on plant roots	$RCF_{S,NPh}$	*	207	270
	RCF_{HPh}		374	329
	RCF_{org-N}		49	61
	k_{ads}	1/h	19	57
Microbial growth ***	$\mu_{max,b}$	1/h	0.216	0.027
	$\mu_{max,f}$		0.164	0.236
	$K_{S,R,NPh,b}$	mg/L	32.26	36.12
	$K_{S,R,NPh,f}$		101.19	34.60
	$K_{S,R,Ph,b}$		56.63	78.97
	$K_{S,R,Ph,f}$		82.01	75.31
	$K_{S_i,R,Ph,b}$		23.12	69.32
	$K_{S_i,R,Ph,f}$		129.87	106.28
	$K_{S,in-N,b}$		5.54	0.07
	$K_{S,in-N,f}$		0.01	33.67
	$K_{S,NO_3,b}$		0.49	0.55
	$K_{S,P,b}$		13.35	0.10
	$K_{S,P,f}$		22.61	0.60
Enzymatic decomposition ***	n_h	-	1.90	1.79
	$k_{dec,\ S,NPh,b}$	**	10.75	18.04
	$k_{dec,\ S,NPh,f}$		72.73	25.57
	$k_{dec,HPh,\ b}$		1.02	2.11
	$k_{dec,HPh,f}$		12.56	18.25
	k_{ammon}		65.80	203.21
Phosphorus precipitation	k_{prec}	1/h	0.377	0.595

* (mg-substrate/kg-root tissue)/(mg/L), ** mg-substrate/g-biomass h, *** *b* and *f* indicators in parameter symbols account for bacterial and fungal biomass, correspondingly.

Table A5. Sensitivity coefficients of σ of the calibrated parameters for both pilot units.

Related Process	Parameter	Pilot Unit	
		P. granatum	***M. communis***
Plant uptake	$TSCF_{R,NPh}$	0.0067	0.0063
	$TSCF_{LPh}$	0.0037	0.0019
	$TSCF_{in-N}$	0.0127	0.0139
	$TSCF_{org-N}$	0.0028	0.0008
	$TSCF_{P}$	0.0002	0.0090
Adsorption on plant roots	$RCF_{S,NPh}$	0.0036	0.0030
	RCF_{HPh}	0.0031	0.0027
	RCF_{org-N}	0.0142	0.0085
	k_{ads}	0.0001	0.0001
Microbial growth	$\mu_{max,b}$	0.0165	0.0392
	$\mu_{max,f}$	0.0445	0.0247
	$K_{S,R,NPh,b}$	0.0038	0.0043
	$K_{S,R,NPh,f}$	0.0044	0.0032
	$K_{S,R,Ph,b}$	0.0005	0.0006
	$K_{S,R,Ph,f}$	0.0004	0.0006
	$K_{S_i,R,Ph,b}$	0.0004	0.0002
	$K_{S_i,R,Ph,f}$	0.0004	0.0001
	$K_{S,in-N,b}$	0.0170	0.0005
	$K_{S,in-N,f}$	0.0004	0.0183
	$K_{S,NO_3,b}$	0.0001	0.0001
	$K_{S,P,b}$	0.0299	0.0076
	$K_{S,P,f}$	0.0327	0.0121
Enzymatic decomposition	n_h	0.0000	0.0000
	$k_{dec,\ S,NPh,b}$	0.0016	0.0021
	$k_{dec,\ S,NPh,f}$	0.0024	0.0032
	$k_{dec,HPh,\ b}$	0.0011	0.0003
	$k_{dec,HPh,f}$	0.0003	0.0019
	k_{ammon}	0.0216	0.0078
Phosphorus precipitation	k_{prec}	0.0587	0.0377

Table A6. Normalized percent variation in COD and TPh removal by changing model sensitive parameters and model inputs.

			COD Removal				TPh Removal			
		Δ (Par.) (%)	**Δ (Plants ET)**		**Δ (Consumption by RSB)**		**Δ (Plants ET)**		**Δ (Consumption by RSB)**	
			P. granatum	***M. communis***	***P. granatum***	***M. communis***	***P. granatum***	***M. communis***	***P. granatum***	***M. communis***
Estimated parameter	k_{prec}	+20	0.06	0.01	−0.33	−0.28	0.06	0.01	−0.41	−0.32
	$\mu_{max,f}$	+20	−0.03	−0.09	0.12	0.82	−0.06	−0.06	0.30	1.28
	$K_{S,P,f}$	+20	0.03	0.01	−0.14	−0.10	0.06	0.01	−0.30	−0.15
	$K_{S,P,b}$	+20	0.02	0.00	−0.03	0.01	0.00	0.00	0.00	0.03
	k_{ammon}	+20	−0.11	-	0.28	-	−0.07	-	0.33	-
	$K_{S,in-N,b}$	+20	0.02	0.00	−0.03	0.00	0.00	0.00	−0.01	0.00
	$k_{S_{in-N,f}}$	+20	0.00	0.06	0.00	−0.61	0.00	0.03	−0.01	−0.91
	$\mu_{max,b}$	+20	−0.04	−0.02	0.06	−0.01	−0.01	0.01	0.01	−0.64
	RCF_{org-N}	+20	0.07	-	−0.17	-	0.04	-	−0.18	-
	$TSCF_{in-N}$	+20	0.02	0.04	−0.04	−0.37	0.01	0.02	−0.04	−0.54
	$TSCF_P$	+20	0.00	0.01	0.00	−0.18	0.00	0.01	0.00	−0.21
Input values related to the plant and soil characteristics	m_{tissue}	+20	−0.03	0.04	−0.17	−0.44	−0.05	0.00	−0.14	−0.73
	$\left(\frac{X_{rhizosphere\ biom}}{X_{bulk\ biom}}\right)_0$	+100	−0.02	−0.01	0.07	0.12	−0.02	0.00	0.11	0.07
	$\left(\frac{X_f}{X_b}\right)_0$	+20	−0.01	−0.01	0.04	0.12	−0.02	−0.01	0.09	0.18
Input values related to the wastewater characteristics	DO	+20	0.00	0.00	0.00	0.01	0.00	0.00	0.01	0.02
	$\left(\frac{C_{HPh}}{C_{HPh}+C_{LPh}}\right)_0$	+20	−0.01	−0.01	−0.01	0.03	−2.70	−2.85	−2.26	−2.36
	$\left(\frac{C_{org-N}}{C_{org-N}+C_{in-N}}\right)_0$	+10	0.12	−0.01	−0.19	0.12	0.02	−0.01	−0.06	0.27
	$\frac{C_{NO_3^- -N}}{C_{in-N}}$	+20	0.00	0.00	0.00	0.00	0.00	0.00	0.00	0.00

References

1. Koutsos, T.M.; Chatzistathis, T.; Balampekou, E.I. A new framework proposal, towards a common EU agricultural policy, with the best sustainable practices for the re-use of olive mill wastewater. *Sci. Total Environ.* **2018**, *622–623*, 942–953. [CrossRef] [PubMed]
2. Santori, F.; Cicalini, A.R. Process of Olive-Mill Wastewater Phytodepuration and Relative. Plant EP1216963 A, 26 June 2002.
3. Bodini, S.F.; Cicalini, A.R.; Santori, F. Rhizosphere dynamics during phytoremediation of olive mill wastewater. *Bioresour. Technol.* **2011**, *102*, 4383–4389. [CrossRef] [PubMed]
4. Petoussi, M.A.; Kalogerakis, N. Olive mill wastewater phytoremediation employing economically important woody plants. *J. Environ. Manag.* **2022**, *302*, 114076. [CrossRef] [PubMed]
5. Garrido Hoyos, S.E.; Martinez Nieto, L.; Camacho Rubio, F.; Ramos Cormenzana, A. Kinetics of aerobic treatment of olive-mill wastewater (OMW) with *Aspergillus terreus*. *Process. Biochem.* **2002**, *37*, 1169–1176. [CrossRef]
6. Beltran, J.; Gonzalez, T.; Garcia, J. Kinetics of the biodegradation of green table olive wastewaters by aerobic and anaerobic treatments. *J. Hazard. Mater.* **2008**, *154*, 839–845. [CrossRef]
7. Achak, M.; Mandi, L.; Ouazzani, N. Removal of organic pollutants and nutrients from olive mill wastewater by a sand filter. *J. Environ. Manag.* **2009**, *90*, 2771–2779. [CrossRef] [PubMed]
8. Günay, A.; Çetin, M. Determination of aerobic biodegradation kinetics of olive oil mill wastewater. *Int. Biodeterior. Biodegrad.* **2013**, *85*, 237–242. [CrossRef]
9. Chiavola, A.; Farabegoli, G.; Antonetti, F. Biological treatment of olive mill wastewater in a sequencing batch reactor. *Biochem. Eng. J.* **2014**, *85*, 71–78. [CrossRef]
10. Lissaneddine, A.; Mandi, L.; El Achaby, M.; Mousset, E.; Rene, E.R.; Ouazzani, N.; Pons, M.-N.; Aziz, F. Performance and dynamic modeling of a continuously operated pomace olive packed bed for olive mill wastewater treatment and phenol recovery. *Chemosphere* **2021**, *280*, 130797. [CrossRef]
11. Allaoui, S.; Bennani, M.N.; Ziyat, H.; Qabaqous, O.; Tijani, N.; Ittobane, N.; Hodaifa, G. Valorization of crude olive stone in the removing of polyphenols from crude olive mill wastewater: Kinetic, isotherm and mechanism study. *Heliyon* **2021**, *7*, e07525. [CrossRef]
12. Elayadi, F.; Boumya, W.; Achak, M.; Chhiti, Y.; Ezzahrae, F.; Alaoui, M.; Barka, N.; El Adlouni, C. Experimental and modeling studies of the removal of phenolic compounds from olive mill wastewater by adsorption on sugarcane bagasse. *Environ. Chall.* **2021**, *4*, 100184. [CrossRef]
13. Vuppala, S.; Bavasso, I.; Stoller, M.; Di Palma, L.; Vilardi, G. Olive mill wastewater integrated purification through pre-treatments using coagulants and biological methods: Experimental, modelling and scale-up. *J. Clean. Prod.* **2019**, *236*, 117622. [CrossRef]
14. Ciggin, A.S.; Iravanian, A.; Dogruel, S.; Orhon, D. Co-metabolism of olive mill wastewater in sequencing batch reactor under aerobic conditions after Fenton-based oxidation. *J. Water Process. Eng.* **2021**, *43*, 102277. [CrossRef]
15. Vlyssides, A.; Mai, S.; Barampouti, E.M. An integrated mathematical model for co-composting of agricultural solid wastes with industrial wastewater. *Bioresour. Technol.* **2009**, *100*, 4797–4806. [CrossRef] [PubMed]
16. Vasiliadou, I.A.; Muktadirul Bari Chowdhury, A.K.M.; Akratos, C.S.; Tekerlekopoulou, A.G.; Pavlou, S.; Vayenas, D.V. Mathematical modeling of olive mill waste composting process. *Waste Manag.* **2015**, *43*, 61–71. [CrossRef] [PubMed]
17. Fezzani, B.; Ben Cheikh, R. Extension of the anaerobic digestion model No. 1 (ADM1) to include phenol compounds biodegradation processes for simulating the anaerobic co-digestion of olive mill wastes at mesophilic temperature. *J. Hazard. Mater.* **2009**, *162*, 1563–1570. [CrossRef]
18. Kumar, J.L.G.; Zhao, Y.Q. A review on numerous modeling approaches for effective, economical and ecological treatment wetlands. *J. Environ. Manag.* **2011**, *92*, 400–406. [CrossRef]
19. Emerman, S.H. The tipping bucket equations as a model for macropore flow. *J. Hydrol.* **1995**, *171*, 23–47. [CrossRef]
20. Brown, H.; Carrick, S.; Müller, K.; Thomas, S.; Sharp, J.; Rogerio, C.; Holzworth, D.; Clothier, B. Modelling soil-water dynamics in the rootzone of structured and water-repellent soils. *Comput. Geosci.* **2018**, *113*, 33–42. [CrossRef]
21. Vymazal, J.; Kröpfelová, L. Removal of organics in constructed wetlands with horizontal sub-surface flow: A review of the field experience. *Sci. Total Environ.* **2009**, *407*, 3911–3922. [CrossRef]
22. Muktadirul Bari Chowdhury, A.K.M.; Akratos, C.S.; Vayenas, D.V.; Pavlou, S. Olive mill waste composting: A review. *Int. Biodeterior. Biodegrad.* **2013**, *85*, 108–119. [CrossRef]
23. Tsagaraki, E.; Lazarides, H.N.; Petrotos, K.B. Chapter 8—Olive Mill Wastewater Treatment. In *Utilization of by-Products and Treatment of Waste in the Food Industry*, 1st ed.; Oreopoulou, V., Winfried, R., Eds.; Springer: New York, NY, USA, 2007; pp. 133–157.
24. El-Abbassi, A.; Saadaoui, N.; Kiai, H.; Raiti, J.; Hafidi, A. Potential applications of olive mill wastewater as biopesticide for crops protection. *Sci. Total Environ.* **2017**, *576*, 10–21. [CrossRef] [PubMed]
25. McNamara, C.J.; Anastasiou, C.C.; O'Flaherty, V.; Mitchell, R. Bioremediation of olive mill wastewater. *Int. Biodeterior. Biodegrad.* **2008**, *61*, 127–134. [CrossRef]
26. Torrecilla, J.S. Chapter 40—Phenolic Compounds in Olive Oil Mill Wastewater. In *Olives and Olive Oil Health and Disease Prevention*, 1st ed.; Preedy, V.R., Watson, R.R., Eds.; Academic Press: Cambridge, MA, USA, 2010; pp. 357–365.
27. Regni, L.; Gigliotti, G.; Nasini, L.; Agrafioti, E.; Galanakis, C.M.; Proietti, P. Chapter 5—Reuse of Olive Mill Waste as Soil Amendment. In *Olive Mill Waste-Recent Advances for Sustainable Management*, 1st ed.; Galanakis, C.M., Ed.; Elsevier Inc.: Amsterdam, The Netherlands, 2017; pp. 97–117.

28. Piotrowska, A.; Rao, M.A.; Scotti, R.; Gianfreda, L. Changes in soil chemical and biochemical properties following amendment with crude and dephenolized olive mill waste water (OMW). *Geoderma* **2011**, *161*, 8–17. [CrossRef]
29. Mechri, B.; Cheheb, H.; Boussadia, O.; Attia, F.; Ben Mariem, F.; Braham, M.; Hammami, M. Effects of agronomic application of olive mill wastewater in a field of olive trees on carbohydrate profiles, chlorophyll a fluorescence and mineral nutrient content. *Environ. Exp. Bot.* **2011**, *71*, 184–191. [CrossRef]
30. Víctor-Ortega, M.D.; Ochando-Pulido, J.M.; Hodaifa, G.; Martinez-Ferez, A. Final purification of synthetic olive oil mill wastewater treated by chemical oxidation using ion exchange: Study of operating parameters. *Chem. Eng. Process.* **2014**, *85*, 241–247. [CrossRef]
31. Kotsou, M.; Mari, I.; Lasaridi, K.; Chatzipavlidis, I.; Balis, C.; Kyriacou, A. The effect of olive oil mill wastewater (OMW) on soil microbial communities and suppressiveness against *Rhizoctonia solani*. *Appl. Soil Ecol.* **2004**, *26*, 113–121. [CrossRef]
32. Blagodatskaya, E.; Kuzyakov, Y. Mechanisms of real and apparent priming effects and their dependence on soil microbial biomass and community structure: Critical review. *Biol. Fertil. Soils* **2008**, *45*, 115–131. [CrossRef]
33. Belaqziz, M.; Tan, S.P.; El-Abbassi, A.; Kiai, H.; Hafidi, A.; O'Donovan, O.; McLoughlin, P. Assessment of the antioxidant and antibacterial activities of different olive processing wastewaters. *PLoS ONE* **2017**, *12*, e0182622. [CrossRef]
34. Dermeche, S.; Nadour, M.; Larroche, C.; Moulti-Mati, F.; Michaud, P. Olive mill wastes: Biochemical characterizations and valorization strategies. *Process. Biochem.* **2013**, *48*, 1532–1552. [CrossRef]
35. Asses, N.; Ayed, L.; Bouallagui, H.; Sayadi, S.; Hamdi, M. Biodegradation of different molecular-mass polyphenols derived from olive mill wastewaters by *Geotrichum candidum*. *Int. Biodeterior. Biodegrad.* **2009**, *63*, 407–413. [CrossRef]
36. Aresta, M.; Acquaviva, M.I.; Baruzzi, F.; Lo Noce, R.M.; Matarante, A.; Narracci, M.; Stabili, L.; Cavallo, R.A. Isolation and characterization of polyphenols-degrading bacteria from olive-mill wastewaters polluted soil. *World J. Microbiol. Biotechnol.* **2010**, *26*, 639–647. [CrossRef]
37. Karakaya, A.; Laleli, Y.; Takaç, S. Development of process conditions for biodegradation of raw olive mill wastewater by *Rhodotorula glutinis*. *Int. Biodeterior. Biodegrad.* **2012**, *75*, 75–82. [CrossRef]
38. Aquilanti, L.; Taccari, M.; Bruglieri, D.; Osimani, A.; Clementi, F.; Comitini, F.; Ciani, M. Integrated biological approaches for olive mill wastewater treatment and agricultural exploitation. *Int. Biodeterior. Biodegrad.* **2014**, *88*, 162–168. [CrossRef]
39. Daâssi, D.; Lozano-Sánchez, J.; Borrás-Linares, I.; Belbahri, L.; Woodward, S.; Zouari-Mechichi, H.; Mechichi, T.; Nasri, M.; Segura-Carretero, A. Olive oil mill wastewaters: Phenolic content characterization during degradation by *Coriolopsis gallica*. *Chemosphere* **2014**, *113*, 62–70. [CrossRef] [PubMed]
40. García García, I.; Jiménez Peña, P.R.; Bonilla Venceslada, J.L.; Martín Martín, A.; Martín Santos, M.A.; Ramos Gómez, E. Removal of phenol compounds from olive mill wastewater using *Phanerochaete chrysosporium*, *Aspergillus niger*, *Aspergillus terreus* and *Geotrichum candidum*. *Process. Biochem.* **2000**, *35*, 751–758. [CrossRef]
41. Salgado, J.M.; Abrunhosa, L.; Venâncio, A.; Domínguez, J.M.; Belo, I. Combined bioremediation and enzyme production by *Aspergillus* sp. in olive mill and winery wastewaters. *Int. Biodeterior. Biodegrad.* **2016**, *110*, 16–23. [CrossRef]
42. Henze, M.; Gujer, W.; Mino, T.; van Loosdrecht, M. *ActivatedSludge Models ASM1, ASM2, ASM2d, and ASM3*, 1st ed.; IWA Publishing: London, UK, 2000.
43. Zhao, Q.; Thompson, A.M.; Callister, S.J.; Tfaily, M.M.; Bell, S.L.; Hobbie, S.E.; Hofmockel, K.S. Dynamics of organic matter molecular composition under aerobic decomposition and their response to the nitrogen addition in grassland soils. *Sci. Total Environ.* **2022**, *806*, 150514. [CrossRef]
44. Kapellakis, I.; Tzanakakis, V.A.; Angelakis, A.N. Land application-based olive mill wastewater management. *Water* **2015**, *7*, 362–376. [CrossRef]
45. Mekki, A.; Dhouib, A.; Sayadi, S. Polyphenols dynamics and phytotoxicity in a soil amended by olive mill wastewaters. *J. Environ. Manag.* **2007**, *84*, 134–140. [CrossRef]
46. Cardinali, A.; Cicco, N.; Linsalata, V.; Minervini, F.; Pati, S.; Pieralice, M.; Tursi, N.; Lattanzio, V. Biological activity of high molecular weight phenolics from olive mill wastewater. *J. Agric. Food Chem.* **2010**, *58*, 8585–8590. [CrossRef] [PubMed]
47. Borja, R.; Alba, J.; Banks, C.J. Impact of the main phenolic compounds of olive mill wastewater (OMW) on the kinetics of acetoclastic methanogenesis. *Process. Biochem.* **1997**, *32*, 121–133. [CrossRef]
48. Pirt, S.J. Maintenance energy: A general model for energy-limited and energy-sufficient growth. *Arch. Microbiol.* **1982**, *133*, 300–302. [CrossRef]
49. Karpouzas, D.G.; Ntougias, S.; Iskidou, E.; Rousidou, C.; Papadopoulou, K.K.; Zervakis, G.I.; Ehaliotis, C. Olive mill wastewater affects the structure of soil bacterial communities. *Appl. Soil Ecol.* **2010**, *45*, 101–111. [CrossRef]
50. Mekki, A.; Dhouib, A.; Sayadi, S. Changes in microbial and soil properties following amendment with treated and untreated olive mill wastewater. *Microbiol. Res.* **2006**, *161*, 93–101. [CrossRef] [PubMed]
51. Di Serio, M.G.; Lanza, B.; Mucciarella, M.R.; Russi, F.; Iannucci, E.; Marfisi, P.; Madeo, A. Effects of olive mill wastewater spreading on the physico-chemical and microbiological characteristics of soil. *Int. Biodeterior. Biodegrad.* **2008**, *62*, 403–407. [CrossRef]
52. Zuthi, M.F.R.; Guo, W.S.; Ngo, H.H.; Nghiem, L.D.; Hai, F.I. Enhanced biological phosphorus removal and its modeling for the activated sludge and membrane bioreactor processes. *Bioresour. Technol.* **2013**, *139*, 363–374. [CrossRef]
53. Weihrauch, C.; Opp, C. Ecologically relevant phosphorus pools in soils and their dynamics: The story so far. *Geoderma* **2018**, *325*, 183–194. [CrossRef]

54. Reichenauer, T.G.; Germida, J.J. Phytoremediation of organic contaminants in soil and groundwater. *ChemSusChem* **2008**, *1*, 708–717. [CrossRef]
55. Zhang, C.; Feng, Y.; Liu, Y.; Chang, H.; Li, Z.; Xue, J. Uptake and translocation of organic pollutants in plants: A review. *J. Integr. Agric.* **2017**, *16*, 1659–1668. [CrossRef]
56. Schachtman, D.P.; Reid, R.J.; Ayling, S.M. Phosphorus Uptake by Plants: From Soil to Cell. *Plant Physiol.* **1998**, *116*, 447–453. [CrossRef] [PubMed]
57. Reid, R.; Hayes, J. Mechanisms and control of nutrient uptake in plants. *Int. Rev. Cytol.* **2003**, *229*, 73–114. [PubMed]
58. Manzoni, S.; Molini, A.; Porporato, A. Stochastic modelling of phytoremediation. *Proc. R. Soc. A* **2011**, *467*, 3188–3205. [CrossRef]
59. Briggs, G.G.; Bromilow, R.H.; Evans, A.A. Relationships Between Lipophilicity and Root Uptake and Translocation of Non-ionised Chemicals by Barley. *Pestic. Sci.* **1982**, *13*, 495–504. [CrossRef]
60. Hopmans, J.W.; Bristow, K.L. Current Capabilities and Future Needs of Root Water and Nutrient Uptake Modeling. *Adv. Agron.* **2002**, *77*, 103–183.
61. Hussain, I.; Aleti, G.; Naidu, R.; Puschenreiter, M.; Mahmood, Q.; Rahman, M.M.; Wang, F.; Shaheen, S.; Syed, J.H.; Reichenauer, T.G. Microbe and plant assisted-remediation of organic xenobiotics and its enhancement by genetically modified organisms and recombinant technology: A review. *Sci. Total Environ.* **2018**, *628–629*, 1582–1599. [CrossRef] [PubMed]
62. U.S. Enviromental Protection Agency. *Introduction to Phytoremediation*; EPA/600/R-99/107; U.S. Environmental Protection Agency: Washington, DC, USA, 2000; pp. 1–72.
63. Marathe, R.A.; Chaudhary, D.T.; Shinde, Y.R. Roots density and activity of pomegranate grown in light textured soil of semi-arid region. *Vegetos* **2017**, *30*, 48–50. [CrossRef]
64. Finzi, A.C.; Abramoff, R.Z.; Spiller, K.S.; Brzostek, E.R.; Darby, B.A.; Kramer, M.A.; Phillips, R.P. Rhizosphere processes are quantitatively important components of terrestrial carbon and nutrient cycles. *Glob. Chang. Biol.* **2015**, *21*, 2082–2094. [CrossRef]
65. Englezos, P.; Kalogerakis, N. *Applied Parameter Estimation for Chemical Engineers*, 1st ed.; CRC Press: Boca Raton, FL, USA, 2000; pp. 79–81.
66. Tziotzios, G.; Lyberatos, G.; Pavlou, S.; Vayenas, D.V. Modelling of biological phenol removal in draw-fill reactors using suspended and attached growth olive pulp bacteria. *Int. Biodeterior. Biodegrad.* **2008**, *61*, 142–150. [CrossRef]
67. Aggelis, G.; Iconomou, D.; Christou, M.; Bokas, D.; Kotzailias, S.; Christou, G.; Tsagou, V.; Papanikolaou, S. Phenolic removal in a model olive oil mill wastewater using *Pleurotus ostreatus* in bioreactor cultures and biological evaluation of the process. *Water Res.* **2003**, *37*, 3897–3904. [CrossRef]
68. Ahmadi, M.; Vahabzadeh, F.; Bonakdarpour, B.; Mofarrah, E.; Mehranian, M. Application of the central composite design and response surface methodology to the advanced treatment of olive oil processing wastewater using Fenton's peroxidation. *J. Hazard. Mater.* **2005**, *B123*, 187–195. [CrossRef]
69. Zhang, Y.; Lashermes, G.; Houot, S.; Doublet, J.; Steyer, J.P.; Zhu, Y.G.; Barriuso, E.; Garnier, P. Modelling of organic matter dynamics during the composting process. *Waste Manag.* **2012**, *32*, 19–30. [CrossRef] [PubMed]
70. Geng, C.; Haudin, C.S.; Zhang, Y.; Lashermes, G.; Houot, S.; Garnier, P. Modeling the release of organic contaminants during compost decomposition in soil. *Chemosphere* **2015**, *119*, 423–431. [CrossRef] [PubMed]
71. Dettenmaier, E.M.; Doucette, W.J.; Bugbee, B. Chemical hydrophobicity and uptake by plant roots. *Environ. Sci. Technol.* **2009**, *43*, 324–329. [CrossRef] [PubMed]
72. Doucette, W.J.; Shunthirasingham, C.; Dettenmaier, E.M.; Zaleski, R.; Fantke, P.; Arnot, J.A. A review of measured bioaccumulation data on terrestrial plants for organic chemicals: Metrics, variability, and the need for standardized measurement protocols. *Environ. Toxicol. Chem.* **2018**, *37*, 21–33. [CrossRef]
73. Kamath, R.; Rentz, J.A.; Schnoor, J.L.; Alvarez, P.J.J. Phytoremediation of hydrocarbon-contaminated soils: Principles and applications. *Stud. Surf. Sci. Catal.* **2004**, *151*, 447–478.
74. Lamshoeft, M.; Gao, Z.; Resseler, H.; Schriever, C.; Sur, R.; Sweeney, P.; Webb, S.; Zillgens, B.; Reitz, M.U. Evaluation of a novel test design to determine uptake of chemicals by plant roots. *Sci. Total Environ.* **2018**, *613–614*, 10–19. [CrossRef]
75. Shone, M.G.T.; Wood, A.V. A comparison of the uptake and translocation of some organic herbicides and a systemic fungicide by barley: I. Absorption in relation to physico-chemical properties. *J. Exp. Bot.* **1974**, *25*, 390–400. [CrossRef]
76. Li, Y.; Chiou, C.T.; Li, H.; Schnoor, J.L. Improved prediction of the bioconcentration factors of organic contaminants from soils into plant/crop roots by related physicochemical parameters. *Environ. Int.* **2019**, *126*, 46–53. [CrossRef]
77. Namiki, S.; Otani, T.; Motoki, Y.; Seike, N.; Iwafune, T. Differential uptake and translocation of organic chemicals by several plant species from soil. *J. Pestic. Sci.* **2018**, *43*, 96–107. [CrossRef]
78. Magdich, S.; Ben Ahmed, C.; Jarboui, R.; Ben Rouina, B.; Boukhris, M.; Ammar, E. Dose and frequency dependent effects of olive mill wastewater treatment on the chemical and microbial properties of soil. *Chemosphere* **2013**, *93*, 1896–1903. [CrossRef] [PubMed]
79. Mekki, A.; Arous, F.; Aloui, F.; Sayadi, S. Nitrogen dynamics in soil amended by Olive Mill Waste Waters and poultry manure codigestate Nitrogen dynamics in soil amended by olive mill waste waters and poultry manure codigestate. *J. Biotech. Phyto.* **2018**, *2*, 1–8.
80. Silva, J.S.; Rego, F.C.; Martins-Loução, M.A. Root distribution of mediterranean woody plants. Introducing a new empirical model. *Plant Biosyst.* **2003**, *137*, 63–72. [CrossRef]

81. Teh, C.B.S. *Introduction to Mathematical Modeling of Crop Growth: How the Equations are Derived and Assembled into a Computer Program*, 1st ed.; Brown Walker Press: Boca Raton, FL, USA, 2006; pp. 111–114.
82. Kendy, E.; Gerard-Marchant, P.; Walter, M.T.; Zhang, Y.; Liu, C.; Steenhuis, T.S. A soil-water-balance approach to quantify groundwater recharge from irrigated cropland in the North China Plain. *Hydrol. Process.* **2003**, *17*, 2011–2031. [CrossRef]
83. Fredlund, D.G.; Rahardjo, H.; Fredlund, M.D. *Unsaturated Soil Mechanics in Engineering Practice*, 1st ed.; John Wiley & Sons, Inc.: Hoboken, NJ, USA, 2012; pp. 274–277.
84. Green, S.R.; Kirkham, M.B.; Clothier, B.E. Root uptake and transpiration: From measurements and models to sustainable irrigation. *Agric. Water Manag.* **2006**, *86*, 165–176. [CrossRef]
85. Peters, A. Modified conceptual model for compensated root water uptake—A simulation study. *J. Hydrol.* **2016**, *534*, 1–10. [CrossRef]
86. Fredlund, D.G.; Xing, A. Equations for the soil-water characteristic curve. *Can. Geotech. J.* **1994**, *31*, 521–532. [CrossRef]
87. Corapcioglu, M.Y. *Advances in Porous Media*; Elsevier Science B.V.: Amsterdam, The Netherlands, 1996; Volume 3, pp. 52–62.
88. Hu, Q.; Wang, J.S.Y. Aqueous-phase diffusion in unsaturated geologic media: A review. *Crit. Rev. Environ. Sci. Technol.* **2003**, *33*, 275–297. [CrossRef]
89. Lugli, F.; Mahler, C.F. A soil-plant model applied to phytoremediation of metals. *Int. J. Phytoremediation* **2016**, *18*, 295–307. [CrossRef]
90. Garcia, H.E.; Gordon, L.I. Oxygen solubility in seawater: Better fitting equations. *Limnol. Oceanogr.* **1992**, *37*, 1307–1312. [CrossRef]
91. Benson, B.B.; Krause, D., Jr. The concentration and isotopic fractionation of oxygen dissolved in freshwater and seawater in equilibrium with the atmosphere. *Limnol. Oceanogr.* **1984**, *29*, 620–632. [CrossRef]
92. Van De Werf, H.; Verstraete, W. Estimation of active soil microbial biomass by mathematical analysis of respiration curves: Calibration of the test procedure. *Soil Biol. Biochem.* **1987**, *19*, 253–260. [CrossRef]
93. Smith, O.L. An analytical model of the decomposition of soil organic matter. *Soil Biol. Biochem.* **1979**, *11*, 585–606. [CrossRef]
94. Sole-Mauri, F.; Illa, J.; Magrí, A.; Prenafeta-Boldú, F.X.; Flotats, X. An integrated biochemical and physical model for the composting process. *Bioresour. Technol.* **2007**, *98*, 3278–3293. [CrossRef]
95. D'Antuono, I.; Kontogianni, V.G.; Kotsiou, K.; Linsalata, V.; Logrieco, A.; Tasioula-Margari, M.; Cardinali, A. Polyphenolic characterization of olive mill wastewaters, coming from Italian and Greek olive cultivars, after membrane technology. *Food Res. Int.* **2014**, *65*, 301–310. [CrossRef]
96. Moraetis, D.; Stamati, F.E.; Nikolaidis, N.P.; Kalogerakis, N. Olive mill wastewater irrigation of maize: Impacts on soil and groundwater. *Agric. Water Manag.* **2011**, *98*, 1125–1132. [CrossRef]
97. Tsiknia, M.; Tzanakakis, V.A.; Oikonomidis, D.; Paranychianakis, N.V.; Nikolaidis, N.P. Effects of olive mill wastewater on soil carbon and nitrogen cycling. *Appl. Microbiol. Biotechnol.* **2014**, *98*, 2739–2749. [CrossRef]
98. Kaczmarek, W. A comparison of bacterial and fungal biomass in several cultivated soils. *Acta Microbiol. Pol.* **1984**, *33*, 239–247.
99. Rawls, W.J.; Brakensiek, D.L.; Saxton, K.E. Estimation of soil water properties. *Trans. ASAE* **1982**, *25*, 1316–1320, 1328. [CrossRef]
100. Šimůnek, J.; Hopmans, J.W. Modeling compensated root water and nutrient uptake. *Ecol. Modell.* **2009**, *220*, 505–521. [CrossRef]
101. Albasha, R.; Mailhol, J.C.; Cheviron, B. Compensatory uptake functions in empirical macroscopic root water uptake models—Experimental and numerical analysis. *Agric. Water Manag.* **2015**, *155*, 22–39. [CrossRef]
102. Yang, D.; Zhang, T.; Zhang, K.; Greenwood, D.J.; Hammond, J.P.; White, P.J. An easily implemented agro-hydrological procedure with dynamic root simulation for water transfer in the crop-soil system: Validation and application. *J. Hydrol.* **2009**, *370*, 177–190. [CrossRef]
103. Heinen, M. Compensation in Root Water Uptake Models Combined with Three-Dimensional Root Length Density Distribution. *Vadose Zone J.* **2014**, *13*, 1–9. [CrossRef]